DSX 18 (2024) 103111

Contents lists available at ScienceDirect

Diabetes & Metabolic Syndrome: Clinical Research & Reviews

journal homepage: www.elsevier.com/locate/dsx

Exploring the therapeutic targets of stevioside in management of type 2 diabetes by network pharmacology and *in-silico* approach

Amit Dutta [a], Md. Arju Hossain [b], Pratul Dipta Somadder [a], Mahmuda Akter Moli [c], Kawsar Ahmed [d,e,f,*], Md Masuder Rahman [a,**], Francis M. Bui [e]

[a] Department of Biotechnology and Genetic Engineering, Mawlana Bhashani Science and Technology University, Tangail, 1902, Bangladesh
[b] Department of Microbiology, Primeasia University, Banani, Dhaka, 1213, Bangladesh
[c] Department of Pharmaceuticals and Industrial Biotechnology, Sylhet Agricultural University, Bangladesh
[d] Department of Information and Communication Technology, Mawlana Bhashani Science and Technology University (MBSTU), Santosh, Tangail, 1902, Bangladesh
[e] Department of Electrical and Computer Engineering, University of Saskatchewan, 57 Campus Drive, Saskatoon, SK, S7N 5A9, Canada
[f] Health Informatics Research Lab, Department of Computer Science and Engineering, Daffodil International University, Daffodil Smart City (DSC), Birulia, Savar, Dhaka, 1216, Bangladesh

ARTICLE INFO

Keywords:
Stevioside
T2D
PTGS2
PPARG
Molecular docking
Molecular dynamics simulation

ABSTRACT

Aims: The main objective of the current study is to investigate the pathways and therapeutic targets linked to stevioside in the management of T2D using computational approaches.
Methods: We collected RNA-seq datasets from NCBI, then employed GREIN to retrieve differentially expressed genes (DEGs). Computer-assisted techniques DAVID, STRING and NetworkAnalyst were used to explore common significant pathways and therapeutic targets associated with T2D and stevioside. Molecular docking and dynamics simulations were conducted to validate the interaction between stevioside and therapeutic targets.
Results: Gene ontology and KEGG analysis revealed that prostaglandin synthesis, IL-17 signaling, inflammatory response, and interleukin signaling were potential pathways targeted by stevioside in T2D. Protein-protein interactions (PPI) analysis identified six common hub proteins (*PPARG*, *PTGS2*, *CXCL8*, *CCL2*, *PTPRC*, and *EDN1*). Molecular docking results showed best binding of stevioside to *PPARG* (−8 kcal/mol) and *PTGS2* (−10.1 kcal/mol). Finally, 100 ns molecular dynamics demonstrated that the binding stability between stevioside and target protein (PPARG and PTGS2) falls within the acceptable range.
Conclusions: This study reveals that stevioside exhibits significant potential in controlling T2D by targeting key pathways and stably binding to *PPARG* and *PTGS2*. Further research is necessary to confirm and expand upon these significant computational results.

1. Introduction

Type 2 diabetes (T2D) is a pervasive metabolic disorder that has a global impact, affecting a significant number of individuals, and its pervasiveness has been increasing (Candia et al. [1]; Rowley et al. [2]). According to the International Diabetes Federation (IDF) data, the year 2019 witnessed 4.2 million deaths attributed to diabetes, while the number of individuals aged 20 to 79 affected by the condition reached 463 million, with forecasts of 700 million by 2045 (Garcia et al. [3]). T2D is characterized by insufficient insulin levels due to dysfunctional pancreatic β-cells and insulin resistance in target organs (Chen et al. [4]). Chronic low-grade inflammation is a significant factor in the progression of insulin resistance and beta-cell dysfunction in T2D (Zatterale et al. [5]). Moreover, it arises due to hereditary factors and lifestyle choices like inadequate physical activity, tobacco smoking, and excessive alcohol consumption (Gupta et al. [6]; Zheng et al. [7]). Research suggests that oxidative stress is a major factor in the development of insulin resistance and T2D. Recently, *PPARG*, *PTGS2*, *TCF7L2*, *CDKAL1*, *IGF2BP2*, *SLC30A8*, *JAZF1*, and *HHEX* are genes strongly linked to the development of T2D (Reddy et al. [8]; Olokoba et al. [9]). Glycemic management can postpone or avoid T2D consequences, according to the United Kingdom Prospective Diabetes Study (UKPDS) (Beigi et al. [10];

* Corresponding author. Department of Information and Communication Technology, Mawlana Bhashani Science and Technology University (MBSTU), Santosh, Tangail, 1902, Bangladesh.
** Corresponding author.
E-mail addresses: kawsar.ict@mbstu.ac.bd, k.ahmed@usask.ca (K. Ahmed), masudmbstu@gmail.com (M.M. Rahman).

https://doi.org/10.1016/j.dsx.2024.103111
Received 16 December 2023; Received in revised form 17 July 2024; Accepted 24 August 2024
Available online 27 August 2024

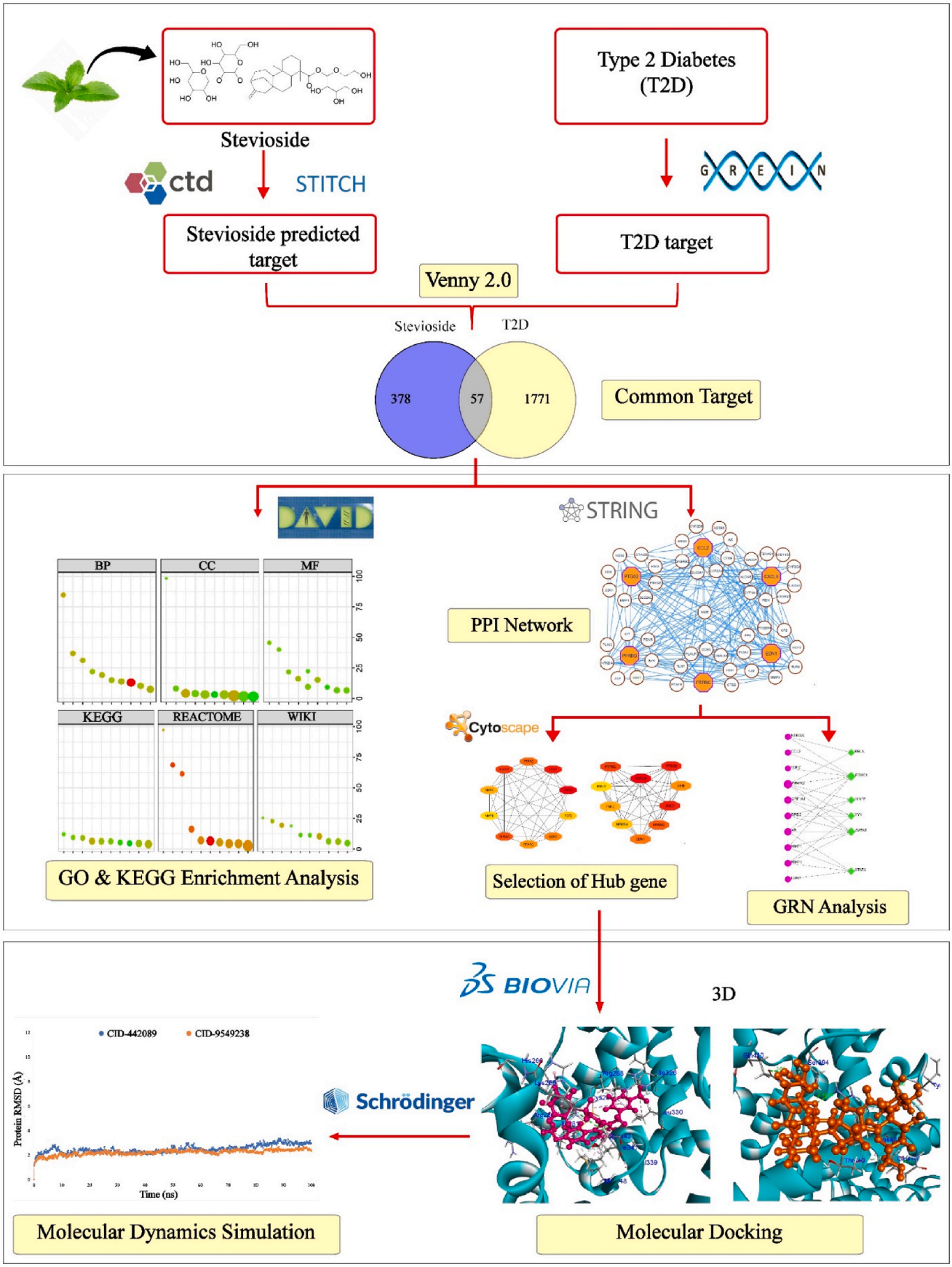

Fig. 1. Workflow for stevioside in the management of T2D.

Gæde et al. [11]). T2D leads to significant complications affecting the cardiovascular system, ocular structures, renal function, and peripheral nerves (Yang et al. [12]; Schalkwijk et al. [13]).

Several chemical medicines have been formulated to control and treat T2D effectively, with metformin being recognized as the primary medication of choice. Metformin influences insulin sensitivity, promoting enhanced glucose uptake within the hepatic tissue (Foretz et al. [14]). A class of antihyperglycemic drug thiazolidinediones (TZDs) such as rosiglitazone and pioglitazone, specifically target and activate the peroxisome proliferator-activated receptor gamma (*PPARG*), enhancing insulin sensitivity and glucose metabolism in T2D (Nanjan et al. [15]). However, existing pharmaceutical therapies cannot provide a complete cure and most chemical therapies are costly and have side effects. Thus, natural phytochemicals could serve as a major alternative for managing T2D, mitigating current therapy limitations. Several plants like *Siraitia grosvenorii* commonly known as monk fruit, contain natural non-nutritive sweeteners that lower blood glucose (Tey et al. [16]). Some *in-vitro*, *in-vivo*, and human studies found that phytochemicals, especially stevioside and several steviol glycoside have antihyperglycemic effects in humans and rodents (Eddouks et al. [17]).

Stevia rebaudiana is an herbaceous perennial plant that contains diterpenic steviol glycosides, notably stevioside and rebaudioside A, which are the most abundant compound. For over a century, the utilization of the stevia plant, its extracts, and stevioside as natural zero-calorie sweeteners has been observed in South America and Asia (Ilić et al. [18]). The joint FAO/WHO expert committee on food additives (JECFA, 2008) determined the safety of steviol glycosides for use in foods and beverages (Sukhmani et al. [19]). The aqueous extract of stevia and stevioside has beneficial effects on pancreatic tissue, including increased insulin levels, antihyperglycemic properties, and antioxidant activity in diabetic rats (Assaei et al. [20]). Additionally, stevioside reduces inflammation by downregulating pro-inflammatory cytokines in mouse (Jeppesen et al. [21]). It exhibits anti-inflammatory effects by inhibiting the activation of NF-κB in LPS-stimulated macrophages (Potočnjak et al. [22]; Boonkaewwan et al. [23]; Alavala et al. [24]) and reducing the expression of *NLRP3* inflammasome activation and inflammatory protein expression in chondrocytes (Wan et al. [25]). Moreover, stevioside activates the Nrf2 pathway to reduce oxidative stress and protects against TAA-induced liver damage by modulating NF-κB and increasing Nrf2 activity in rats (Hao et al. [26]; Casas-Grajales et al. [27]). Besides, the impact of stevioside on the activity of islet cells closely resembles that of glucagon-like peptide-1 (GLP-1). Study indicates that GLP-1 and stevioside did not induce basal insulin secretion, but both enhanced the release of insulin in response to glucose in mouse islets (Chen et al. [28]). A previous study showed that stevioside modulated blood glucose levels and dose-dependently decreased *PEPCK* gene expression in the liver of rats (Chen et al. [29]). Overall, it has been demonstrated to have positive effects on insulin secretion, glucagon secretion, blood glucose levels, and blood pressure (Ilić et al. [18]).

Previous research has indicated the potential of stevioside in regulating blood glucose levels. However, no therapeutic targets has been extensively studied through integrated bioinformatics and network pharmacology approaches. This study proposes to fill this gap by utilizing RNA-seq datasets to identify differentially expressed genes (DEGs) that are common to both T2D and targets of stevioside. RNA-seq is a reliable and efficient technique for analyzing gene expression at a large scale. Multiple gene expression profiling studies have identified hundreds of DEGs that participate in various molecular functions, biological processes, and signaling pathways. These may be useful as therapeutic targets and diagnostic markers for disease development (Stupnikov et al. [30]). This study retrieved RNA-seq datasets from the Gene Expression Omnibus (GEO) database to identify T2D-associated DEGs and stevioside targets from multiple databases. Based on common targets, further integrated bioinformatics investigation was conducted, including pathway enrichment, locating hub proteins from protein-protein interaction and gene regulatory network analysis. Finally, molecular docking and molecular dynamics simulations were conducted to validate the interaction between stevioside and potential hub targets. Despite of several limitations, this study will reveal novel and significant insights into the molecular mechanism of the antihyperglycemic activity of stevioside, thereby contributing to the field of diabetes research and its management. The framework of the proposed study is illustrated in Fig. 1.

2. Materials and methods

2.1. Stevioside related gene screening

Several databases such as CTD (ctdbase.org/), STITCH (stitch.embl.de/), PharmGKB (www.pharmgkb.org/), PharmMapper (www.lilabecust.cn pharmmapper), Swiss Target prediction (www.swisstargetprediction.ch/), and ChEMBL (www.ebi.ac.uk/chembldb) are used to identify probable targets of stevioside. The comparative toxicogenomics database is a manually curated comprehensive resource that incorporates interactions derived from literature and its purpose is to improve the comprehension of toxicological information about chemicals, diseases, genes, phenotypes, and exposures, thereby augmenting the existing knowledge base related to human health (Davis et al. [31]). The pharmacogenetics knowledge base provides access to phenotype, genomic, and clinical data from ongoing pharmacogenetic studies (Hewett et al. [32]). Since understanding protein-small molecule interactions is crucial for molecular and cellular functions, STITCH integrates crystal structures, binding experiments, metabolic pathways and drug-target relationships for easy access to this data (Kuhn et al. [33]). The PharmMapper online tool is a web server that utilizes reversed pharmacophore matching to identify potential drug targets (Wang et al. [34]). Based on a combination of 3D and 2D similarity measurements with established ligands, SwissTargetPrediction server accurately predicts the targets of bioactive molecules (Gfeller et al. [35]). The ChEMBL database provides information on binding, functional features, and ADMET for various of drug-like bioactive chemicals (Gaulton et al. [36]). To improve the validity of the findings and identify potential stevioside targets, we selected all genes from each database.

2.2. T2D related gene screening

To find out the drug target proteins of host, we collected primary data on the gene expression profiling of T2D. The NCBI (https://www.ncbi.nlm.nih.gov/geo/) Gene Expression Omnibus (GEO) data repository was used to retrieve the datasets with the accession number GSE135155 (case = 6 and control = 6), GSE156109 (case = 6 and control = 6), GSE116369 (case = 4 and control = 4), GSE53949 (case = 5 and control = 5), and GSE159984 (case = 20 and control = 20) (Geer et al. [37]). Human Adipocyte tissue and pancreatic β-cells were the sources for generating the RNA-seq datasets involving an equal number of control and case samples. GREIN (GEO RNA-seq Experiments Interactive Navigator) (www.ilincs.org/apps/grein/?gse=) was used to analyze these datasets, which offers intuitive interfaces for manipulating and comprehensive analysis of gene expression signatures through subsetting, visualization, and statistical power analysis (Kaussner et al. [38]).

2.3. Analysis of differentially expressed genes

We relied on publicly available RNA-Seq data for this investigation. Numerous statistical processes were first performed on the datasets to determine the differentially expressed genes (DEGs). Additionally, to achieve a balance between the identification of statistically significant genes and to control results that are false positives, the Benjamini-Hochberg false discovery rate technique is employed. Quantile standardization and Z-score transformation were used to standardize gene expression data for the disease and control condition to avoid

Table 1
A summary of datasets is presented with geo-features and quantitative data.

GSE number	Source name	Control sample	Case sample	DEGs	Up	Down
GSE135155	Adipocyte tissue	6	6	500	441	59
GSE156109	Pancreatic β-cell	6	6	548	322	226
GSE116369	Beta cell	4	4	421	248	173
GSE53949	Pancreatic islet	5	5	422	201	221
GSE159984	Pancreatic β-cell	20	20	330	164	166

experimental system issues. To further exclude possible sources of error from our data, we performed an ANOVA test to measure the degree of statistical relevance between groups (Rahman et al. [39]). These studies determined DEGs with the absolute value of log folds change >1 and an absolute P-value <0.05. Then sorting the upregulated and down-regulated DEGs assuming logFC >1 and logFC < -1 accordingly. Venny 2.0 (https://bioinfogp.cnb.csic.es/tools/venny/index.html) (Oliveros [40]) webserver was used to understand the distribution of significant DEGs across the datasets.

2.4. Functional enrichment analysis

We inferred the signaling pathways (KEGG, WiKi, and Reactome) and gene ontologies, i.e. biological process (BP), molecular function (MF) and cellular components (CC) related to the frequent DEGs using several databases. The analysis of overrepresentation revealed several functional Gene Ontology (GO) keywords and enriched cell signaling pathways, which provide evidence for the biological relevance of the identified DEGs. The present research delineates the roles of stevioside's primary target in treating T2D, as GO specifies. The KEGG pathway is an extensively employed resource that functions as a knowledge repository for the examination of biological pathways and cellular processes (Kanehisa [41]). We searched for the DAVID database by inserting the 57 core common targets for GO enrichment and signaling pathway analysis. Then, SRplot (https://www.bioinformatics.com.cn/en) was used to generate the bubble plot for GO enrichment and analysis of signaling pathways.

2.5. Protein-protein interaction analysis

Protein-protein interaction (PPI) refers to the interaction among proteins, that interact to achieve molecular function, biological processes, and cellular components (Shekarappa et al. [42]). The STRING (https://string-db.org/) database generated a PPI network by uploading the common targets related to stevioside and T2D. Cytoscape v3.9.1 was utilized to generate and analyze network profiles (Darbeheshti et al. [43]).

2.6. Analysis of cluster and hub proteins selection

The presentation of clustering results is necessary to analyze of the structural characteristics of biological networks. We utilized the ClusterViz component of Cytoscape 3 to conduct cluster analysis in this study. Out of the three algorithms, we specifically select MCODE (Molecular Complex Detection) to detect proteins with a high degree of interconnectivity. This method utilizes a set of predetermined criteria, which includes a degree score threshold of 2, a node score threshold of 0.2, and a K-Core value of 2 (Wang et al. [44]).

CytoHubba is an open platform for investigating the pivotal hub

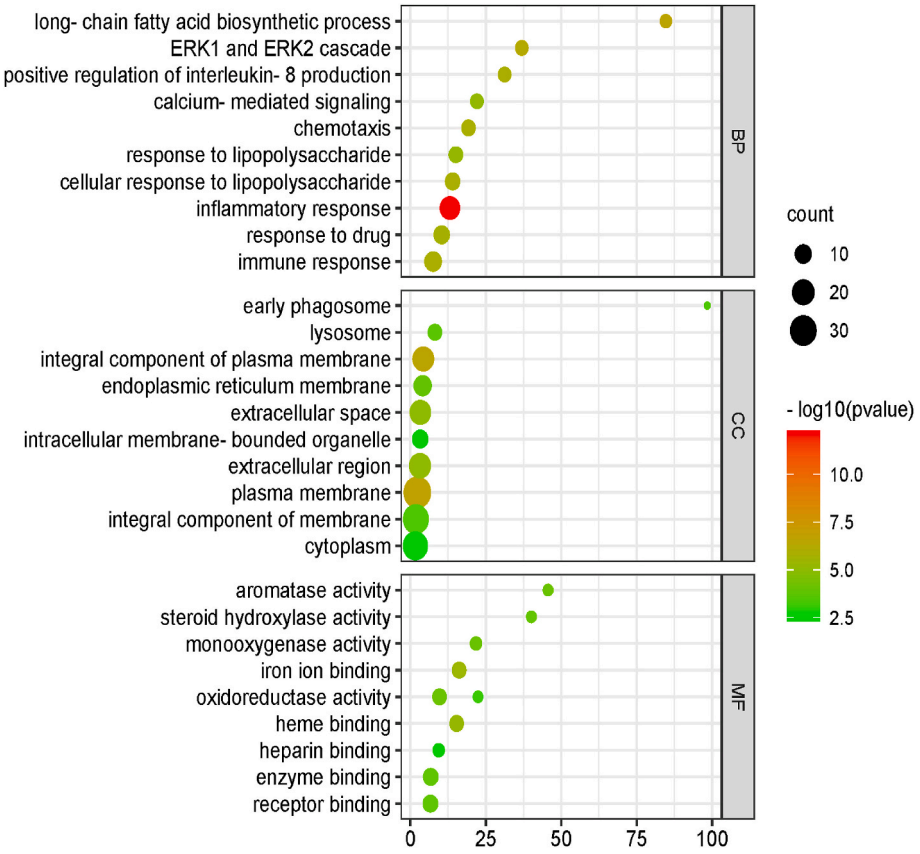

Fig. 2. The bubble plot represents the biological process (BP), cellular component (CC), and molecular function (MF) analyses of the differentially expressed genes (DEGs) in T2D. The combined score (P-value) was used to sort the results of the pathway terms.

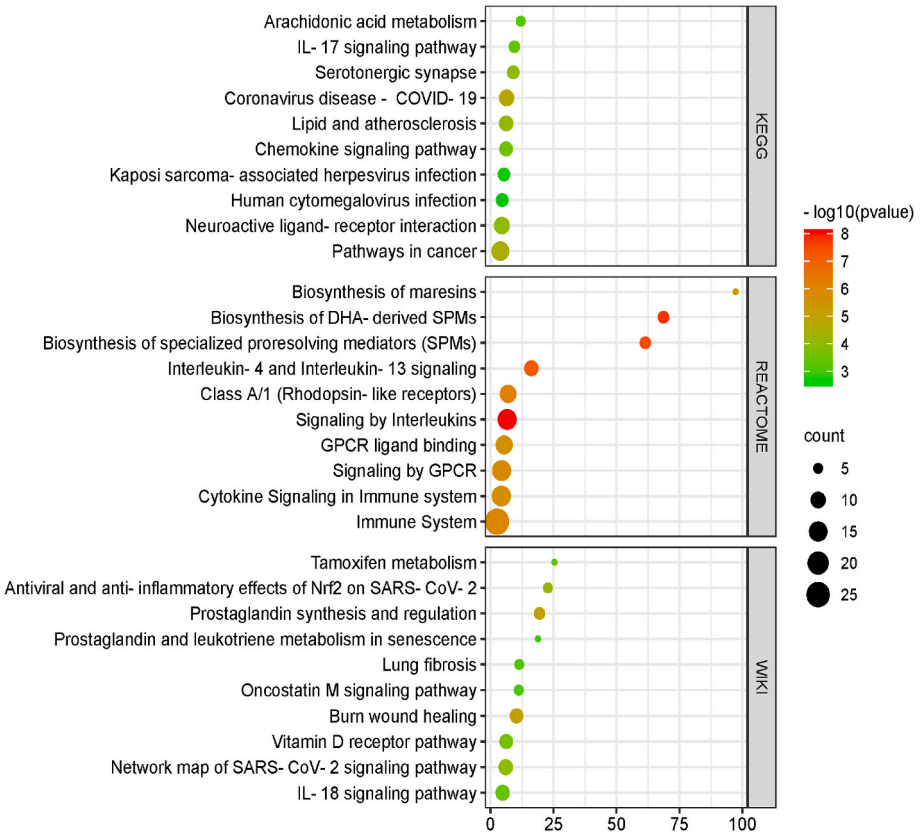

Fig. 3. The bubble plot represents the signaling pathways associated with the differentially expressed genes (DEGs) in T2D, based on the KEGG, Reactome and Wiki database. The combined score (P-value) was used to sort the results of the pathway terms.

proteins involved in the subnetwork (Chin et al. [45]). We employed five different methods from the CytoHubba plugin: degree, MNC, MCC, betweenness, and closeness centrality. However, we have listed common hub proteins comparing five cytoHubba methods using the jVenn online server (https://jvenn.toulouse.inrae.fr/app/index.html) that manages up to six lists of inputs and displays outcomes using either conventional or Edwards-Venn layouts (Bardou et al. [46]).

2.7. Gene regulatory network analysis

Gene regulatory network (GRN) illustrates the impact of molecular regulators on mRNA and protein levels, with transcription factors (TFs) and microRNAs playing crucial roles as gene regulators (Zhou et al. [47]). The TFs and hub genes interaction network is an undirected graph, where nodes represent TFs and edges reflect interactions. Most edges connecting a TF-node to hub genes indicate that it is a key regulator of hub gene regulation; hence, this node is given priority. To identify the most important TFs linked to hub genes, we conducted a network analysis of TFs-hub genes interactions using the JASPAR (Fornes et al. [48]) and Encode (Sloan et al. [49]) databases. Key miRNAs that influence hub genes post-transcriptionally were identified by analyzing miRNAs-hub genes interactions with the TarBase (Papadopoulos et al. [50]) and mirTarBase (Hsu et al. [51]) databases implementing NetworkAnalyst (https://www.network analyst.ca) online server. This web server supports tissue-specific, gene regulatory, co-expression, and toxicogenomics studies and allows users to customize networks and create data analysis projects (Zhou et al. [47]). The hub gene regulators were selected as the top miRNAs and TFs based on their high topological degree and betweenness score. These regulators were chosen to reflect the common enriched TFs and miRNAs, ensuring the credibility of the findings.

2.8. Molecular docking simulation and visualization of ligand-protein complex

Molecular docking is a valuable method for identifying the binding relationship between a ligand and a protein receptor at the molecular and atomic scale (Guedes et al. [52]). After downloading and processing the PDB format of *CXCL8* (PDB ID: 6XMN), *PPARG* (PDB ID: 2HFP), *PTGST2* (PDB ID: 5IKV), and *PTPRC* (PDB ID: 5FMV) proteins from the RCSB Protein Data Bank (Rose et al. [53]) Biovia Discovery Studio Visualizer was utilized to eliminate co-crystalized ligand molecules, introduce hydrogen atoms, and select protein chains. The energy of each refined PDB structure was minimized using the Swiss PDB Viewer software (Guex et al. [54]). The active site of the *CXCL8*, *PPARG*, *PTGST2*, and *PTPRC* was confirmed before the molecular docking simulation study through CASTp (Tian et al. [55]). The 3D structure of stevioside was retrieved from the PubChem database (Kim et al. [56]) and subsequently converted from SDF to PDB format using Biovia Discovery Studio Visualizer 20.1.0 (Nivetha et al. [57]). Co-crystalized ligand molecules were obtained as control ligands from each PDB structure. A molecular docking simulation was performed using AutoDock Vina through PyRx 0.8 virtual screening software. This software utilizes a Lamarckian genetic algorithm along with grid-based energy estimation. To assess the accuracy of the docking software, we conducted re-docking of the co-crystal bound ligand (Dallakyan et al. [58]). For simulating the most effective interaction, the docking was executed by positioning center at coordinates x: 1.7322, y: 18.1636, z: 66.6794 with the dimension in coordinates x: 74.8521, y-75.4757, z-66.6794 Å together with the exhaustiveness equaling to 8. The software comprises AutoDock and AutoDock Vina, utilizing the Lamarckian genetic algorithm as a scoring function. AutoDock tools offer a range of techniques for analyzing docking simulation data, including assessing conformational similarity, visualizing the binding site and its energy, and determining

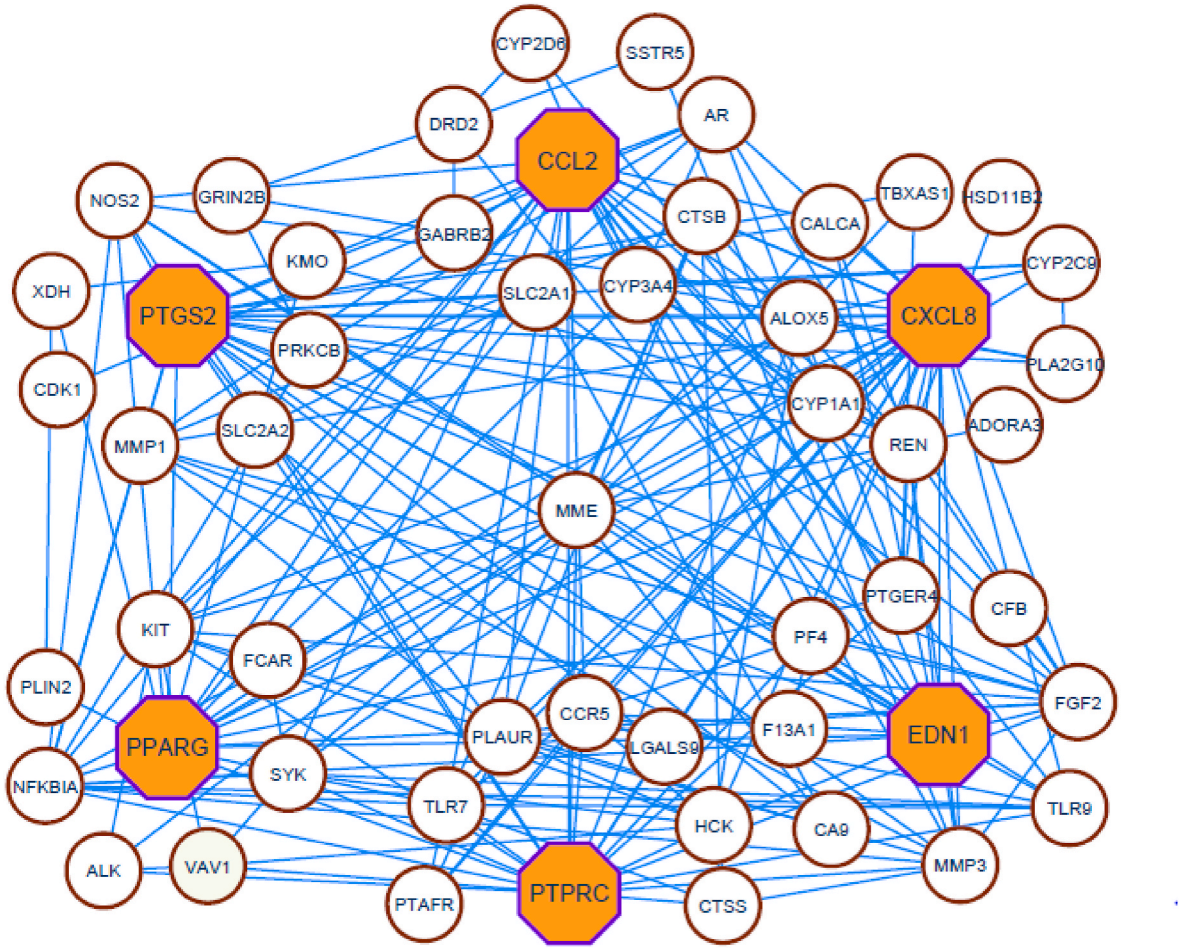

Fig. 4. The PPI network visualizes stevioside's potential therapeutic targets for controlling T2D. The nodes of the network represent target proteins, while the edges represent protein-protein relationships.

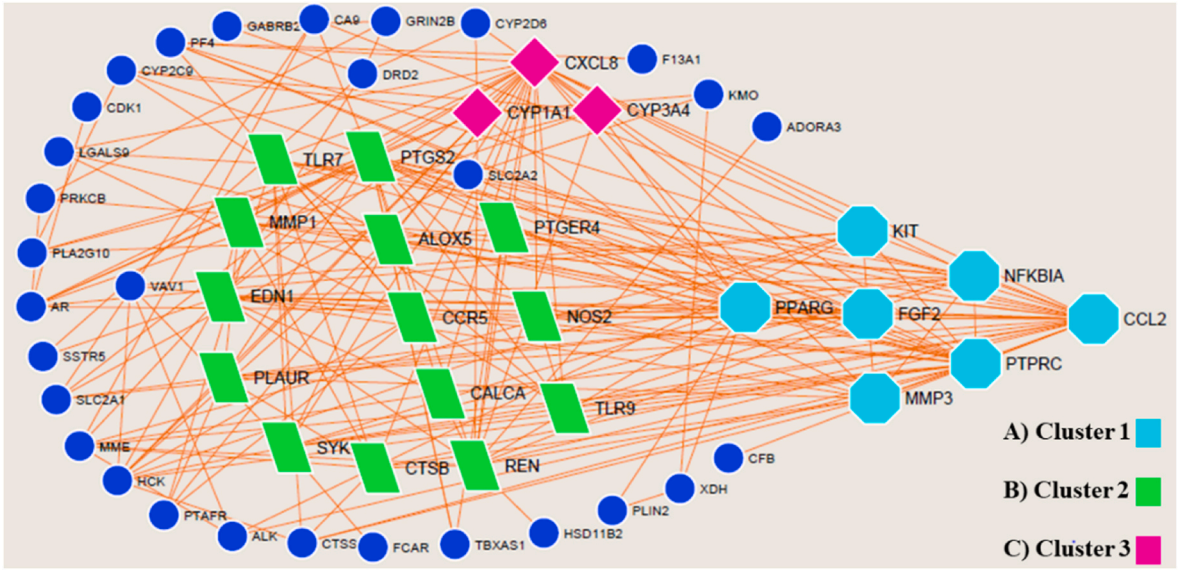

Fig. 5. Indicates (A) cluster 1, (B) cluster 2, and (C) cluster 3 in the PPI network obtained by cluster analysis of the PPI network using Clusterviz in Cytoscape. Blue-colored circles indicate others proteins that mostly don't interconnect.

parameters such as intermolecular energy and inhibition constant. The AutoDock 4.2 scoring tool created and evaluated eight optimal poses for each ligand. The compounds exhibiting lowered binding energy compared to the reference molecule were selected for further analysis. Finally, the 2D and 3D structure and binding interactions were visualized through Biovia Discovery Studio Visualizer 20.1.0 (Nivetha et al.

Table 2
Clustering PPI network data using MCODE.

Cluster	Density Score of Node	Nodes	Edges	Node IDs
C1	5.333	7	32	*NFKBIA, PPARG, KIT, FGF2, MMP3, PTPRC, CCL2*
C2	4.462	14	58	*PTGER4, CCR5, CTSB, TLR9, CALCA, SYK, TLR7, ALOX5, NOS2, EDN1, PTGS2, PLAUR, REN, MMP1*
C3	2	3	4	*CYP1A1, CYP3A4, CXCL8*

[57]).

2.9. Molecular dynamics simulation (MDS)

A 100 ns molecular dynamics simulation (MDS) was performed to evaluate the binding consistency of protein-ligand complex structures. Schrödinger's "Desmond v3.6 Programme" (https://www.schrodinger.com/) was utilized within a Linux framework to conduct the molecular dynamic simulations and assess different protein-ligand complex structures (Arefin et al. [59]; Biswas et al. [60]). The complex molecule was hydrated using a system builder module with a TIP3P hydration model. The hydration was done in a 3D orthorhombic box with a buffer distance of 10 Å. The system was neutralized with counter ions, and the concentration of physiological salt (Na^+ and Cl^-) was limited to 0.15 M. Following that, the structure was refined by optimizing hydrogen bonds and using the OPLS3e force field for energy reduction. OPLS3e enhances the precision of small-molecule conformational tendencies, solvation, and the performance of protein-ligand binding benchmarks (Roos et al. [61]). Isothermal-isobaric ensembles (NPT) gathering, that made utilization of its entire Nose-Hoover thermal variations and associated isotropic methodology, being maintained around 300 K and one atmospheric compression (1.01325 bar), and this being accompanied via 50 PS grabbing pauses with some efficiency equal 1.2 kcal/mol. MD simulation was evaluated using a simulations interaction diagram (SID) within their Desmond components of the Schrödinger suite. The durability of the protein-ligand complex combination was evaluated by analyzing protein-ligand interactions (P-L), the radius of gyration (Rg), and intramolecular hydrogen bond data (Rahman et al. [62]). The proposed RMSD about an MD simulation with the interval during x could be calculated utilizing the power source given the following calculation:

$$\mathrm{RMSD_x} = \sqrt{\frac{1}{\mathrm{N}}\sum_{i=1}^{N}\left(r'i\left(\mathrm{t_x}\right)\right) - \mathrm{r_i}\left(\mathrm{t_{ref}}\right)^2}$$

Where the $RMSD_x$ represents the calculation for a frame x; N is the quantity of atoms chosen; t_{ref} denotes the benchmark duration, and r' represent the position of its chosen atom within frame x, after aligning it with the reference frame, where frame x is recorded at time t_x.

The RMSF for a residue i is calculated by the following calculation:

$$\mathrm{RMSF_i} = \sqrt{\frac{1}{T}\sum_{t=1}^{T} < \left(r'i\left(\mathrm{t}\right)\right) - \mathrm{r_i}\left(\mathrm{tref}\right)^2 >}$$

In this particular case, T stands for the calculated trajectories duration that was utilized to calculate the calculated RMSF. Diagonal parentheses indicate these circular distances mean being calculated throughout the set for residue molecules, using t_{ref} signifying its benchmark duration, r_i its placement for residues i, as well as r' represents the position of atoms in residue i after they have been superimposed on the reference.

2.9.1. Simulation trajectory analysis

The subsequent MD simulation images were made with Schrödinger's maestro program, version 9.5. The proposed model's environment utilized overall simulation interaction diagram (SID) from its Desmond modules in the Schrödinger suite to evaluate overall MD simulation's correctness. Within alignment several parameters including root-mean-square deviation (RMSD), the radius of gyration (Rg), protein-ligand contacts (P-L) and intramolecular hydrogen bonding can be assessed for the equilibrium of the protein-ligand complex.

2.10. Binding free energies analysis from post MDS trajectory

Applying the molecular mechanics of the generalized born and surface area (MM/GBSA) solvation approach was employed to calculate the binding free energies of ligands to the protein. The estimation of the binding free energy using the MM/GBSA method was conducted as follows. The equation ΔGbind = Gcomplex − Greceptor − Gligand is a mathematical representation of the binding free energy. The term ΔGbind represents a difference in free energy between the complex and the combined free energies of the receptor and the ligand. The ΔGbind for the examined complexes was determined using Schrödinger's thermal MM/GBSA script. The MD trajectory is partitioned into distinct frame snapshots and subsequently submitted to MM/GBSA analysis. The reported values represent the average expected free energies (ΔGbind) of binding (Khoury et al. [63]).

3. Results

3.1. Stevioside and T2D overlapping targets

An array of bioinformatics analyses were conducted to determine the genes targeted by stevioside and T2D. Accordingly, we searched and detected 501 stevioside-related targets from databases. A total of 435 distinct common targets were identified after screening duplicated targets. We determined 1828 distinct T2D-related targets out of 2221 targets after screening duplicate genes (Table 1). Finally, we identified 57 overlapping targets of stevioside and T2D using Venn diagram tool.

3.2. Gene ontology and pathway enrichment analysis

GO enrichment analysis was conducted on 57 targets, and a total of 289 GO terms with $p < 0.05$ were obtained, including 226 entries of biological process (BP), 23 entries of cellular component (CC), and 40 entries of molecular function (MF). BP includes an inflammatory response, biosynthetic process of long-chain fatty acid, ERK1 and ERK2 cascade, positive regulation of IL-8 production, cellular response to lipopolysaccharide, chemotaxis, immune response, calcium-mediated signaling, and response to drug. CC comprises plasma membrane, integral component of plasma membrane, extracellular space, lysosome, endoplasmic reticulum membrane, integral component of membrane, extracellular region, and intracellular membrane-bounded organelles. MF exhibited iron ion binding, monooxygenase activity, aromatase activity, steroid hydroxylase activity, enzyme binding, oxidoreductase activity, and heparin binding. The top 10 GO terms were visualized and are displayed in (Fig. 2) and details are provided in (Table S1).

The results of KEGG, reactome and wiki pathway enrichment analysis demonstrated that 57 targets were enriched in 167 pathways with adjusted p-value ($P < 0.05$). A bubble plot was generated to represent the top 10 pathways from each database displayed in (Fig. 3) and details provided in (Table S2). 30 pathways were found to be statistically significant mainly involving IL-17 signaling pathway, arachidonic acid metabolism, prostaglandin synthesis and regulation, prostaglandin synthesis and regulation, coronavirus disease, pathways in cancer, lipid and atherosclerosis, serotonergic synapse, neuroactive ligand-receptor interaction, chemokine signaling pathway, immune system, signaling by GPCR, cytokine signaling in the immune system, GPCR ligand binding, antiviral and anti-inflammatory effects of Nrf2 on SARS-CoV-2, vitamin D receptor pathway, IL-18 signaling pathway, and tamoxifen metabolism. The dimensions of the bubble were determined based on

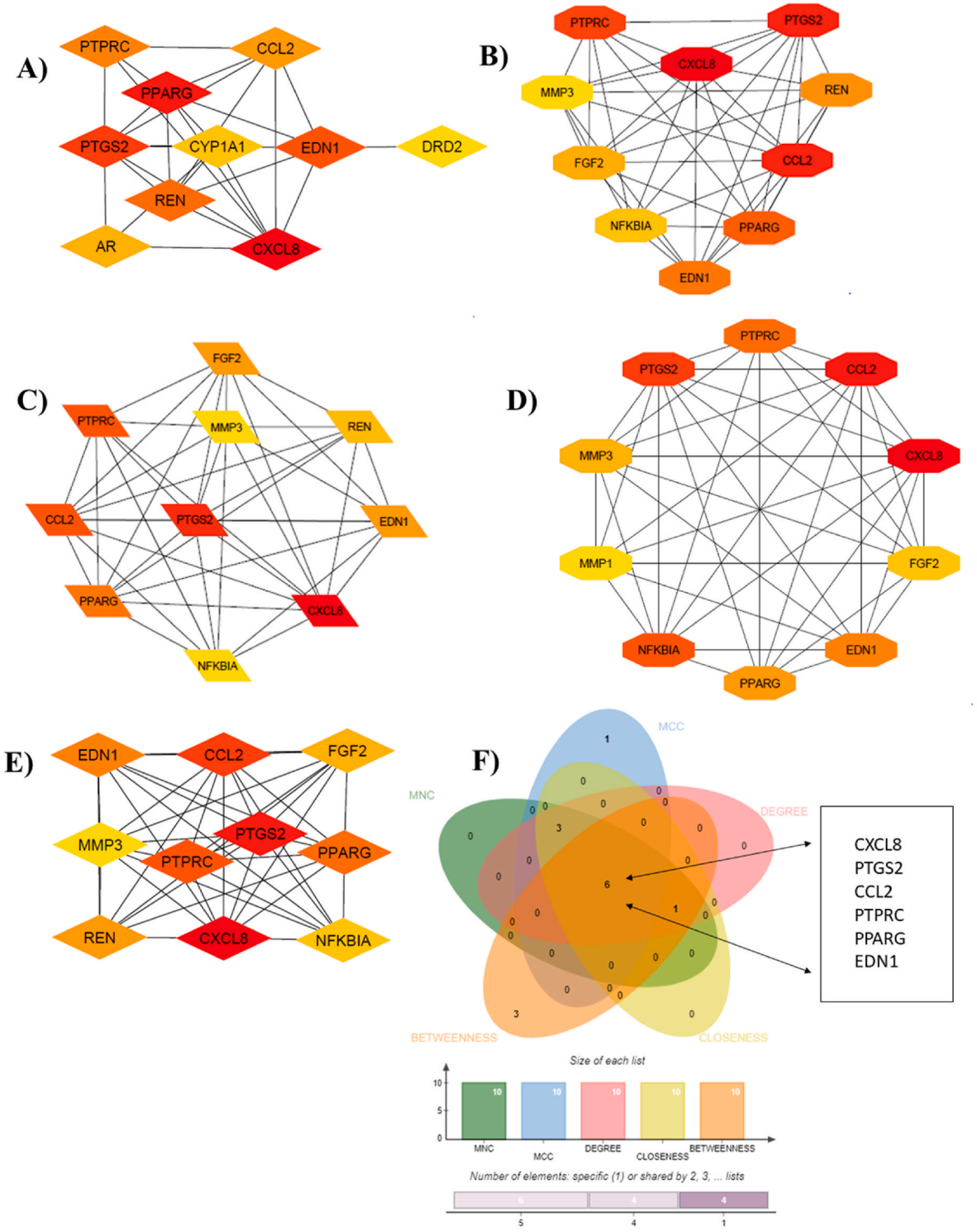

Fig. 6. The network diagram illustrates the primary targets of stevioside in the context of T2D. This analysis used five CytoHubba algorithms: betweenness, degree, MNC, MCC, and closeness (A–E). Moreover, the venn diagram (F) illustrates the presence of six hub proteins that are shared among multiple networks. Red to yellow color gradients indicate the higher to lower significance of reported hub proteins.

the number of associated genes. The color gradient from red to green represents the decrease in p-value and the smaller p-value represents more significant result.

3.3. Protein-protein interaction network construction

A comprehensive understanding of the protein-protein interaction (PPI) network is essential for gaining insights into cell tissue, function, and biological processes. The existence of atypical protein-protein interactions (PPIs) within the interactome of organisms can give rise to various health complications. The current study involved the construction of a PPI network utilizing the 57 common targets shared by stevioside and T2D. The PPI network is comprised of 54 nodes and 210 edges. The present analysis involved the collection of combined scores of

Table 3
Hub proteins emerged from PPI network analysis and presented pathological information of six common hub proteins.

Reference	Hub protein	Description	Pathological role
(Bruun et al. [89])	*CXCL8*	C-X-C motif chemokine ligand 8	Associated with an excessive buildup of intra-abdominal fat leads to T2D.
(Ahmadian et al. [86])	*PPARG*	Peroxisome proliferator-activated receptor gamma	Regulates adipocyte development, lipid metabolism, glucose homeostasis, immune cell metabolism, and inflammation.
(Konheim et al. [79])	*PTGS2*	Prostaglandin endoperoxide synthase 2	Limit glucose-stimulated insulin release and modulate the inflammatory response, decreasing insulin sensitivity.
(Dhananjayan et al. [107])	*EDN1*	Endothelin 1	Contribute to endothelial dysfunction leads to T2D.
(Al Barashdi et al. [108])	*PTPRC*	Receptor-type tyrosine-protein phosphatase C	Need for T cell activation.
(Kim et al. [109])	*CCL2*	C-C Motif Chemokine Ligand 2	Possible role in the recruitment of monocytes into the arterial wall.

the core targets from a STRING database, which were then imported into Cytoscape software to construct the network (Fig. 4).

3.4. Cluster analysis and hub proteins selection

Cluster analysis is commonly employed in exploring significant biological networks like PPI, transcription factor-binding, metabolic, and gene networks. Two prominent modules were identified within the protein-protein interaction network. In Fig. 5, cluster 1 consisted of 7 nodes connected by 32 edges. Similarly, cluster 2 comprised 14 nodes with 58 edges, while a smaller cluster was identified with 3 nodes and 4 edges. Table 2 presents comprehensive information. Hub proteins demonstrate a significant correlation with other proteins within the network, and modifications in their expression can broadly influence the network. It is noteworthy that six hub proteins, namely *CXCL8*, *PTGS2*, *CCL2*, *PTPRC*, *PPARG*, and *EDN1*, were consistently identified in all five methods (Fig. 6). *REN* was found in four methods except MCC and *FGF2*, *NFKBIA*, *MMP3* was found in four methods except betweenness. *AR*, *DRD2*, *MMP1*, *CYP1A1* and *MMP1* are found in betweenness and MCC, respectively. Additionally (Table 3), presents pathological information of six hub proteins.

3.5. Gene regulatory network (GRN) analysis

Gene regulatory analysis of the network involved analyzing the connections between DEGs-TFs, and microRNA-DEGs. Figs. 7 and 8 show the DEGs–miRNA and TFs-DEGs interactions network where the circles represent DEGs, while squares represent miRNAs and TFs. Several transcription factors, namely TFDP1, YY1, HINFP, GATA2, RELA, and STAT3, were identified as the most significant TFs interconnected to hub proteins, based on analysis of the Encode and Jaspar databases. The Tarbase and mirTarbase databases have identified several common miRNAs, such as hsa-mir-124–3p, hsa-mir-21–3p, hsa-mir-1-3p, hsa-mir-101–3p, hsa-mir-155–5p, hsa-mir-210–3p, and hsa-mir-155–5p, hsa-mir-27a-5p. These miRNAs play a significant role as post-transcriptional regulators.

3.6. Binding affinity analysis

The molecular docking study predicted the ability of stevioside to bind to four out of six common hub proteins, as presented in Table 4. The study utilizes docking scores to quantify the chemical-protein binding activity, where the score assesses strength of the molecular interaction. A lower docking score signifies a more stable binding conformation and a stronger molecular interaction. The binding affinities of the four target proteins, *PTGS2* (−10.1 kcal/mol), *PAPRG* (−8 kcal/mol), and *PTPRC*

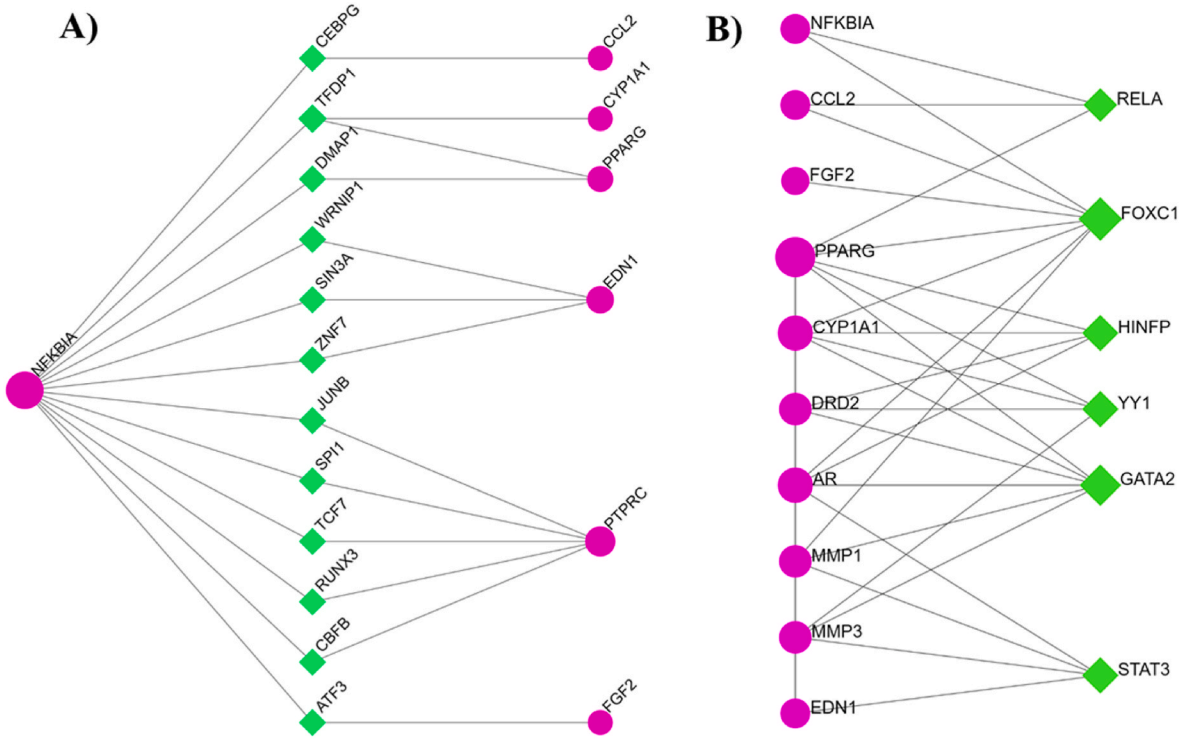

Fig. 7. Gene regulatory network analysis through A) Encode B) Jaspar database. Circular and square shapes indicate the DEGs and transcription factors (TFs).

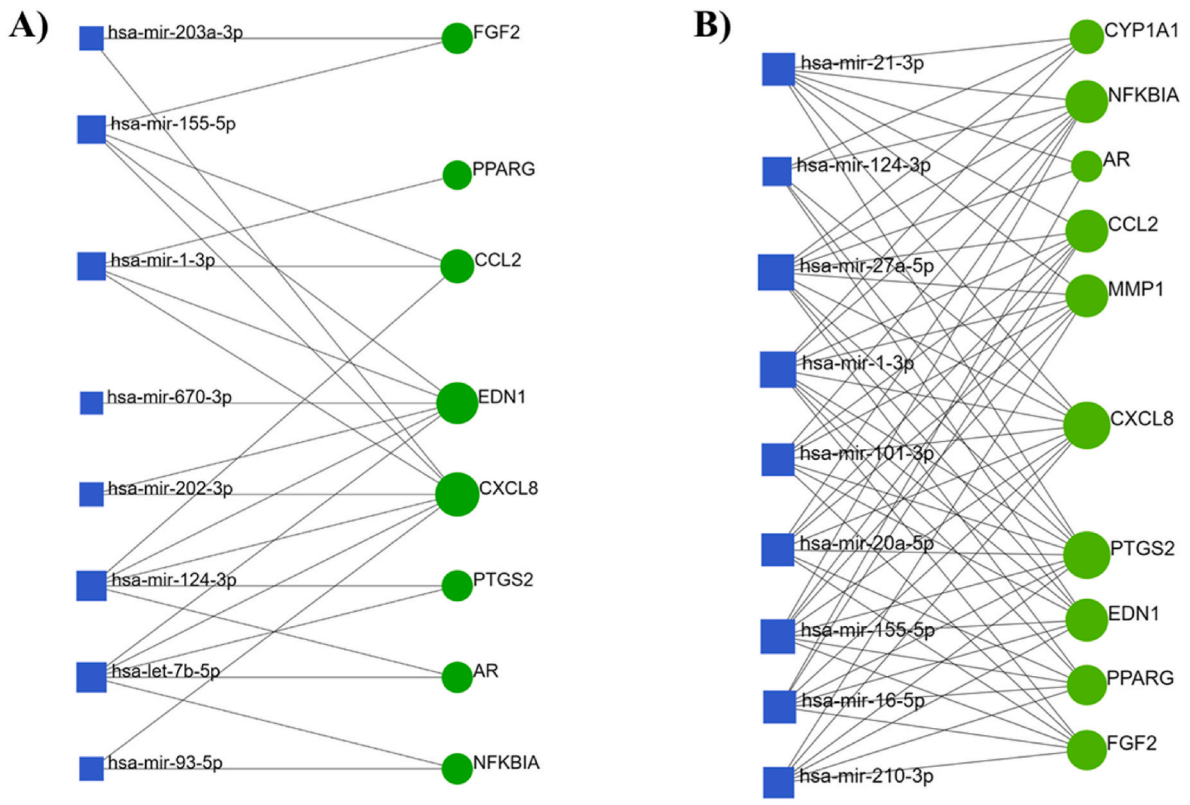

Fig. 8. Gene regulatory network analysis through A) mirTarbase B) Tarbase database. Circular and square shapes indicate the DEGs and mRNA.

(−7.8 kcal/mol), were found to be higher than −7.0 kcal/mol. *CXCL8* showed only (−6.1 kcal/mol) binding affinity with stevioside. *PPARG* protein interacts with GLN A: 444, TYR A: 477, ARG A: 443, SER A: 394, and GLN A: 410 residues through hydrogen bonds and ILE A: 265 HIS A: 266, ILE A: 267, LEU A: 270, ARG A: 288 AND GLU A: 291 residues through hydrophobic bond formation. On the other hand, *PTGS2* interacts with SER A: 143, ASN A: 144, SER A: 146, and GLU A: 236 amino acids for hydrogen bonds and LEU A: 145 LEU A: 224 amino acids for hydrophobic bonds formation. Besides, *PTPRC* interacts with GLN A: 125, and ARG A: 245 residues by forming hydrogen bonds and LEU A: 1215, PHE A: 1290 residues through hydrophobic bonds generation (Fig. 9 and Table 4).

3.7. Molecular dynamics simulation (MDS) trajectory analysis

3.7.1. RMSD analysis

The root mean square deviation (RMSD) in MDS is a metric used to quantify the average distance traveled by a specific atom over a certain period, relative to a reference time frame (Zarezade et al. [64]). The RMSD of the drug candidate compound CID-442089 (stevioside) and the control drug CID- 9549238 complex structure has been evaluated with the *PPARG* (PDB ID: 2HFP) to analyze the alterations in the order in Fig. 10 (A). For *PPARG*, the compound CID-442089 showed a slight upward trend for 1 ns (between 6 and 7 ns) where complexes Cα atoms were within fluctuations range <3 Å. The RMSD curve for the compound was similar to the curve of control. After 87 ns, the compound CID-442089 showed minor fluctuations that were considered acceptable when compared to the structure of the native protein. Similarly, in Fig. 10 (B) the RMSD of drug candidate compound CID-442089 (stevioside) and the control drug CID-3371 with the *PTGS2* (PDB ID: 5IKV) has been calculated. Complexes Cα atoms showed the highest fluctuation at 48ns against compound but overall, the fluctuation range was within 1–3 Å. Overall, the RMSD plot suggests compound CID-442089 is stably bound to *PPARG* and *PTGS2*.

3.7.2. RMSF analysis

In MDS, any local conformational changes experienced by proteins chain are assessed by root mean square fluctuation (RMSF) (Du et al. [65]). These values were evaluated and plotted to compare the flexibility of individual residues in the protein-ligand complexes. During the 100 ns simulation, the protein-RMSF complexes showed minimal variation. A larger RMSF value indicates greater flexibility in the residue, while a lower RMSF value indicates more excellent stability (Zarezade et al. [66]). The C-terminus and N-terminus of a protein and loop regions are more flexible during the MDS than secondary structures and residues that interact with other molecules (Safavi et al. [67]) and so was in this study. The RMSF values of the experimental drug candidate compound CID-442089 (stevioside) and the control drug CID-9549238 bound to *PPARG* (PDB ID: 2HFP) were calculated to assess how ligand attachment affects the flexibility of a specific residue position in the protein structure in Fig. 11 (A). Additionally, Fig. 11 (B) displays the RMSF values of the drug candidate compound CID-442089 (stevioside) and the control drug CID-3371 when interacting with the *PTGS2* protein (PDB ID: 5IKV). For *PPARG*, the RMSF values of most of the remains were identical with a few exceptions. Apart from a few residues, most were less than 2 Å. In the case of *PTGS2*, RMSF values fluctuated reaching a 4.9 Å value for CID-442089. The majority of the residue for compound CID-442089 showed a similar curve with the control drug CID-3371. These RMSF values indicate that binding the ligand did not interfere with the protein structure, which aligns with the RMSD results.

3.7.3. Radius of gyration (Rg) analysis

The Rg value in MDS measures a molecule's compactness level. This measurement estimates the root mean square displacement of the atoms relative to the center of mass. The Rg value is inversely proportional to the compactness of the protein (Safavi et al. [67]). Stability of the drug candidate compound CID-442089 (stevioside) and control CID-9549238 with the target protein was evaluated by analyzing the Rg values during a 100-ns simulation in Fig. 12 (A). The Rg values for the compound

Table 4
Docking results of stevioside and four hub proteins.

Potential target (PDB ID)	Structure of lead compound	Binding affinity (kcal/mol)	Interaction of amino acid	
CXCL8 (6XMN)	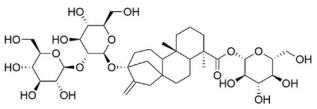 (Stevioside)	−6.1	Hydrogen bond TYR 13, LYS 11, ILE 10, CYS 9, GLN 8, and CYS 50	Hydrophobic bond PHE 17, and LEU 49
PPARG (2HFP)	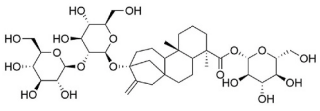 (Stevioside)	−8	GLN 444, TYR 477, ARG 443, SER 394, and GLN 410	LEU 270, HIS 266, LYS265, GLU291, ILE267, and ARG288
PPARG (2HFP)	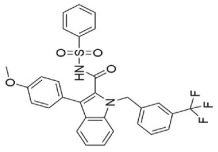 (Control)	−6	LYS 265, SER 342, CYS 285, LEU 330, ARG 288, GLY 284, and ILE 341	HIS 266, ARG 280, ILE 281, MET 348, and VAL 339
PTGS2 (5IKV)	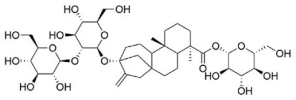 (Stevioside)	−10.1	SER 143, GLU 236, GLU 140, ASN 144, and SER 146	LEU 224, LEU 145, and LEU 145
PTGS2 (5IKV)	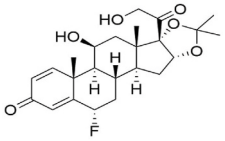 (Control)	−8.2	HIS 386, and HIS 388	PHE 210,and LEU 391
PTPRC (5FMV)	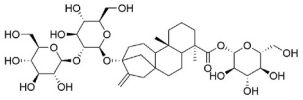 (Stevioside)	−7.8	ARG 245, and GLN 125	PHE 1290, and LEU 1215

CID-442089 (stevioside) and the control CID-9549238 with *PPARG* (PDB ID: 2HFP) were calculated at 6.0 Å and 5.0 Å, suggesting that the binding of the ligand did not create structural alterations in the protein's binding site. Stability of the drug candidate compound CID-442089 (stevioside) and the control drug CID-3371 with the selected protein *PTGS2* (PDB ID: 5IKV) was assessed in Fig. 12 (B). The calculated values were 6.8 Å and 3.7 Å, respectively, indicating that the binding of these ligand compounds does not significantly alter the structure of the protein's binding site.

3.7.4. Evaluation of intramolecular bonds

The stacked bar charts (Fig. 13) depict the duration and characteristics of interactions throughout the course. Receptor-ligand interactions are facilitated via hydrophobic, ionic, hydrogen bonds, and water bridges assigned by different colors in the chart representing these interactions. The y-axis depicts the fraction of residues, whereas the x-axis represents the individual residues. A residue fraction 0.5 indicates that the contact is maintained for 50 % of the simulation time. When combined with the interactions bar chart, the residue interaction diagram provides a comprehensive understanding of the interactions occurring during the simulation (AbdElmoniem et al. [68]). During the 100 ns simulation, an analysis was conducted on the protein complex and its intermolecular interactions with the designated ligands using the Simulation Interactions Diagram (SID). The drug candidate compound CID-442089 (stevioside) and the control drug CID-9549238 interact with the targeted proteins *PPARG* (PDB ID: 2HFP). Compound CID-442089 maintains strong hydrogen bonds with GLU140 (190 %), SER143 (80 %), ASN144 (60 %) of A chain and SER143 (80 %), ASP229 (100 %), GLN241 (90 %) and ARG333 (80 %) of B chain. In the control drug more hydrophobic and water bridge bonds formed with *PTGS2* shown in Fig. 13 (A).

For *PPARG*, compound CID-442089 (stevioside) maintains hydrogen bonds with ASP396 (80 %), THR440 (50 %), and ARG443 (100 %) residue. In addition, it forms hydrophobic interaction with GLU324 (90 %), ASP396 (90 %), MET439 (80 %), and ARG443 (50 %) of *PPARG*. In control drug water bridges, hydrophobic, and hydrogen bonds formed with *PPARG* shown in Fig. 13 (B). These interactions persisted throughout the simulation, facilitating the formation of a stable binding with the target proteins.

3.8. MM/GBSA analysis for binding free energy calculation

The MM/GBSA analysis was employed to calculate the ligand-binding free energy to the protein receptor. The highly negative net binding energies observed in all the docked and control complexes support the formation of strong intermolecular systems and stable complexes. The average binding energies of the complex structures in the case of *PTGS2*, CID-442089 (stevioside) shows higher negative binding free energy −111.55 kcal/mol compared to control −46.55 kcal/mol (Fig. 14 A). Again, the *PPARG* complex shows slightly lower binding energy with CID-442089 (stevioside) −72.88 kcal/mol compared to control −77.46 kcal/mol (Fig. 14 B).

4. Discussion

T2D is a multifaceted disease characterized by a range of health issues and severe complications. While current medications raise safety concerns, it is essential to explore new therapies, including herbal treatments, for effective management of T2D. Previous study showed that phytochemical stevioside is one of the major diterpene glycoside

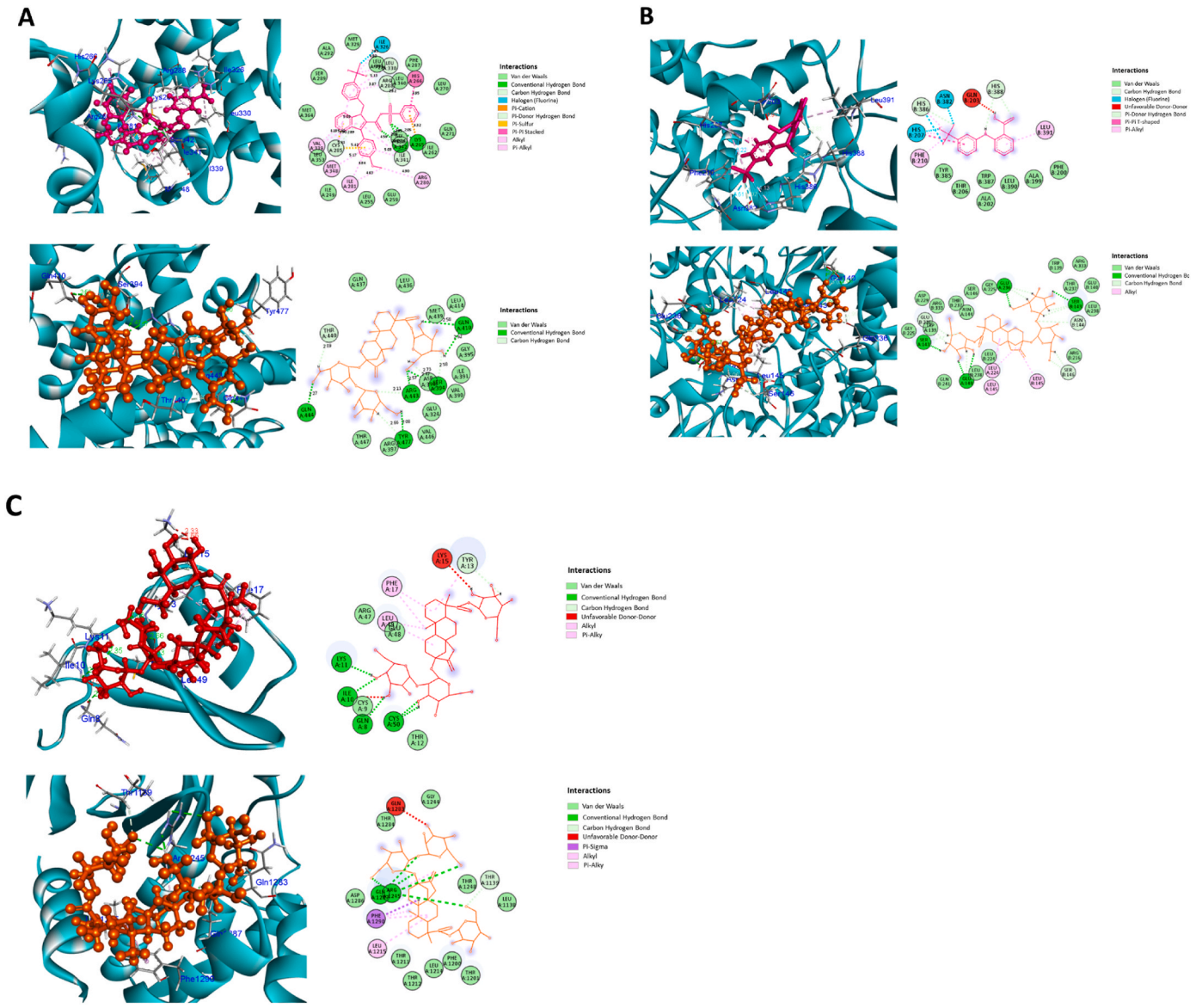

Fig. 9. Binding interaction analysis of hub proteins and stevioside. **(A)** *PPARG* (PDB ID: 2HFP) complex of control (top) and stevioside (bottom); **(B)** *PTGS2* (PDB ID: 5IKV) complex of control (top) and stevioside (bottom) **(C)** *CXCL8* protein (PDB ID: 6XMN) with stevioside (top) and *PTPRC* protein (PDB ID: 5FMV) with stevioside target molecule (bottom).

from the *S. rebaudiana* exhibits insulinotropic, hypoglycemic, and blood pressure-lowering properties (Chen et al. [28]; Sukhmani et al. [18]). In this study, we applied network pharmacology approach and molecular docking to predict and elucidate the potential pathways and therapeutic targets of stevioside against T2D.

In this study, the KEGG, Reactome and Wiki pathways revealed that arachidonic acid metabolism, prostaglandin synthesis and regulation, IL-17 signaling pathway, IL-18 signaling pathway, signaling by interleukins, and atherosclerosis are significant pathways. Arachidonic acid is a potent inducer of insulin secretion however, depending on the cells and tissues involved, its derivatives exhibit varying contributions to insulin resistance (Sonnweber et al. [69]; Luo et al. [70]). *PTGS2* is involved in the metabolism of arachidonic acid to prostaglandin G2. Increased *PTGS2* expression has been observed in islet cells obtained from mouse models of obesity and diabetes, as well as from deceased human organ donors with diabetes. Hence, the beta-cell function is significantly regulated by *PTGS2* and its metabolites (Kimple et al. [71]; Carboneau et al. [72]; Bosma et al. [73]). Our findings revealed that stevioside targets *PTGS2* which is involved in the arachidonic acid metabolism and prostaglandin synthesis pathways. Consequently, targeting this pathway stevioside may control T2D.

A shared molecular framework exists between the inflammatory and insulin signaling pathways, which contribute to the advancement of insulin resistance and endothelial dysfunction. These interconnected processes collectively increase the susceptibility to cardiovascular disorders (Odegaard et al. [74]). Elevated expression of IL-17 through activating the NFkB pathway are linked to the pathophysiology of T2D (Elahi et al. [75]). It is well-recognized that proinflammatory cytokines suppress insulin signaling, resulting in insulin resistance and the emergence of T2D (Moneim et al. [76]). Serum concentrations of IL-18 exhibit a direct correlation with BMI, adiposity, and insulin resistance and remain elevated in newly diagnosed people with T2D (Zaharieva et al. [77]). The serotonergic system contributes substantially to regulating glucose homeostasis playing role in T2D (Iordanidou et al. [78]). This study identified *PPARG, PTGS2, CXCL8, CCL2,* and *EDN1* involved with this significant pathways, and stevioside targets these pathways related to T2D.

Protein-protein interaction and hub proteins were also assessed,

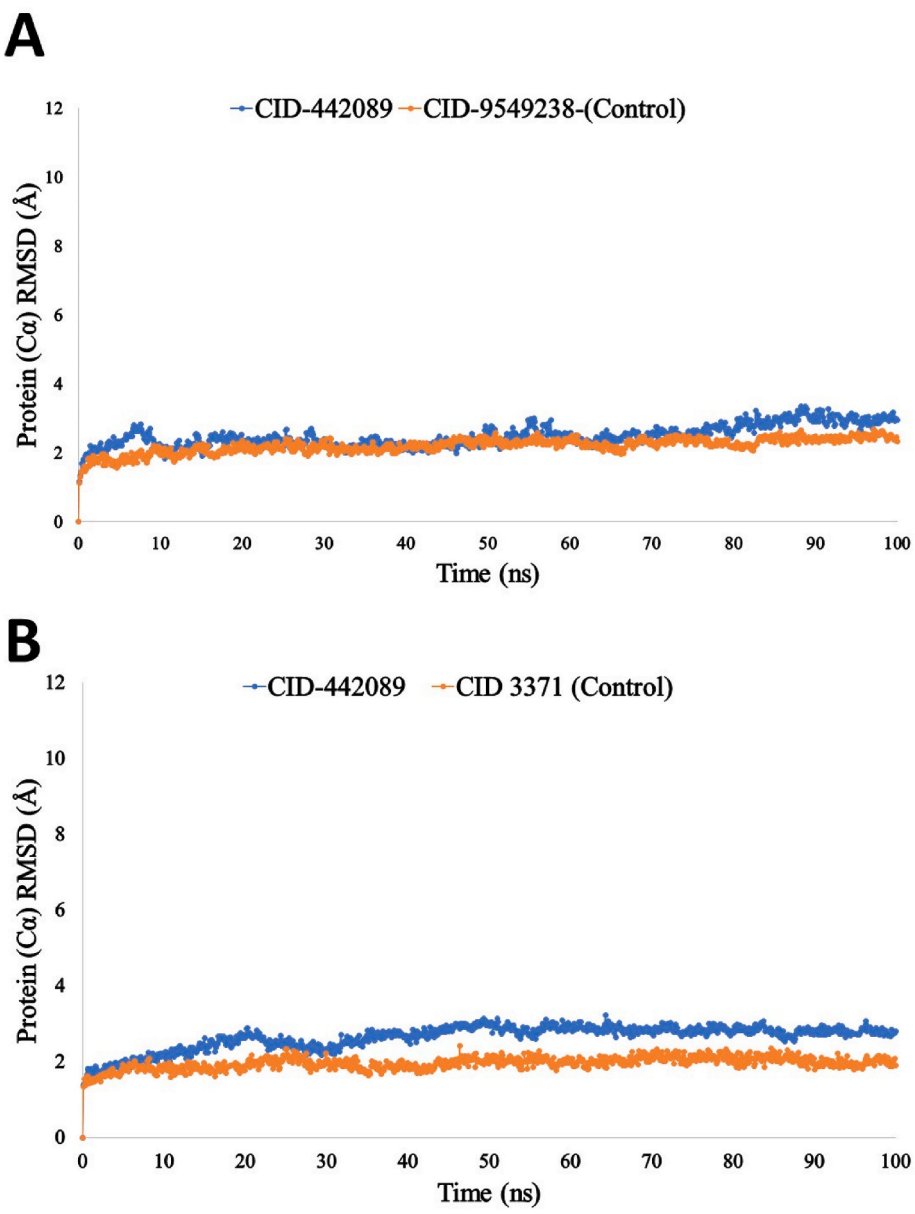

Fig. 10. The RMSD values of 100 ns MDS assessment for the two ligand molecules in complex with the targeted protein (A) CID-442089 (stevioside) with *PPARG* (blue), CID- 9549238 (control) with *PPARG* (orange) and (B) CID-442089 (stevioside) with *PTGS2* (blue), CID- 3371 (control) with *PTGS2* (orange).

where six common hub proteins (*PPARG*, *PTGS2*, *CXCL8*, *CCL2*, *PTPRC*, and *EDN1*) were obtained which commonly played an essential role in the pathogenesis of T2D. Among them, docking studies revealed that stevioside maintains a great binding affinity with *PPARG* and *PTGS2*. Prostaglandin-endoperoxide synthase-2 (*PTGS2*), which makes prostaglandins negatively influence the regulation of glucose-stimulated insulin secretion and act as mediators during the inflammatory response that is linked to insulin resistance (Konheim and Wolford [79]). A study demonstrated that long non-coding RNA *PTGS2* negatively affects the functionality of islet β-cells through its regulation of miR-146a-5p and subsequent upregulation of retinol-binding protein 4 (RBP4) (Chen et al. [80]). In contrast, the administration of stevioside in mice resulted in the inhibition of pro-inflammatory cytokine production and expression of *PTGS2* (Yingkun et al. [81]). Stevioside (10 nM–1 μM), exhibits the capability to diminish the secretion of glucagon. This effect is potentially mediated through an increase in mRNA levels of carnitine palmitoyltransferase, *PPARG*, and stearoyl-CoA desaturase (Hong et al. [82]). Stevioside modulates blood glucose levels by increasing insulin secretion and suppressing PEPCK gene expression in the liver of rats (Chen et al. [29]). This dual mechanism of action leads to reduced plasma glucose levels in diabetic rats, as evidenced by the ability of stevioside to enhance insulin secretion from mouse islets and the β cell line INS-1 (Jeppesen et al. [21]). Again, peroxisome proliferator activated receptor gamma (*PPARG*) plays an important role in lipid and glucose homeostasis (Mal et al. [83]). It regulates the expression of numerous adipose tissue-secreted factors that have a positive or negative effect on insulin sensitivity (Longo et al. [84]). Glucose homeostasis genes, such as glucose transporter type 4 (Glut4) are upregulated by *PPARG* (Wang et al. [85]; Ahmadian et al. [86]). Thiazolidinediones a type of *PPARG* agonist used against T2D, but they have several adverse effects (Lalloyer and Staels [87]). Natural compound stevioside, upregulates *PPARG* by activating the PI3K/AKT signaling pathway, which has been shown to reduce inflammation and neuronal apoptosis in rats (Zhang [88]; Bruun et al. [89]; Straczkowski et al. [90]). These observations enhance the utilization of stevioside in the context of counteracting insulin resistance or enhancing insulin sensitivity in individuals

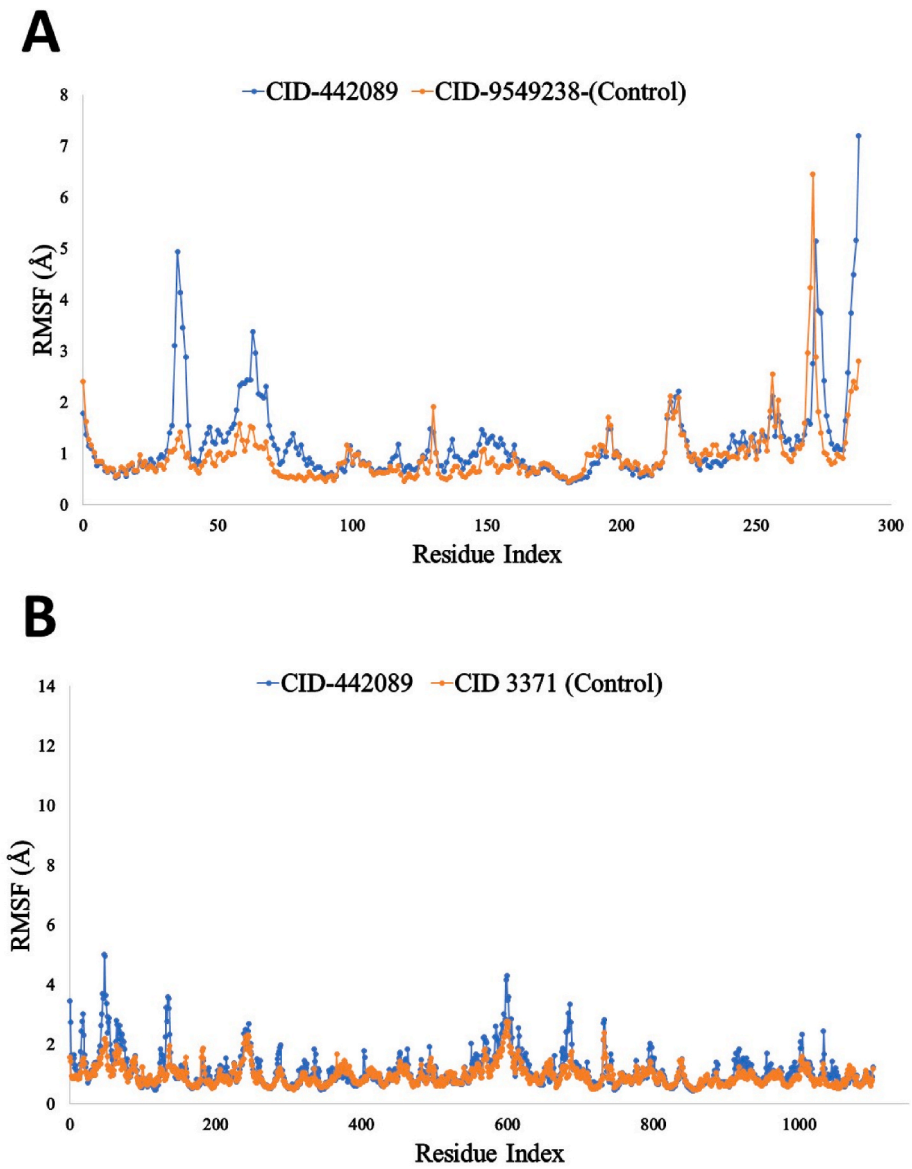

Fig. 11. The RMSF values of 100 ns MDS assessment for the two ligand molecules in complex with the targeted protein (A) CID-442089 (stevioside) with *PPARG* (blue), CID- 9549238 (control) with *PPARG* (orange) and (B) CID-442089 (stevioside) with *PTGS2* (blue), CID- 3371 (control) with *PTGS2* (orange).

with T2D. In this analysis, we predicted that stevioside may target and modulate the *PPARG* and *PTGS2* hub proteins, thus controlling T2D.

In addition, protein tyrosine phosphatase receptor type C (*PTPRC*), also known as CD45, plays a critical role in the development of lymphocytes, the transduction of signals from antigen receptors, and the regulation of signals originating from integrin and cytokine receptors (Hermiston et al. [91]). Protein tyrosine phosphatases are inhibitory regulators of insulin signal transduction in diabetes (Prabhakar et al. [92]). Besides, *CXCL8* induces chemotaxis in its target cells, including T-cells, neutrophil granulocytes, basophils, and adipocytes (Omatsu et al. [93]). Clinical research has suggested that the adipocyte-secreted *CXCL8* may be linked to issues such as T2D, which is associated with an excessive buildup of intra-abdominal fat (Straczkowski et al. [90]). Our result also shows *PTPRC* and *CXCL8* as a key hub protein targeted by stevioside.

Relationships between TFs and DEGs were explored in depth and discovered 18 TFs, of which FOXC1, GATA2, STAT3, and YY1 were significantly enriched and displayed more interactions with DEGs. Researchers found GATA2 may be relevant as a risk factor for coronary artery disease and its key risk factors, including T2D, hypertension (HTN), and dyslipidemia (Muiya et al. [94]). Again, YY1 is a transcriptional activator that plays a role in the expression of the insulin gene. It aids in the maturation and functioning of β-cells following birth (Liu et al. [95]). MicroRNAs have been identified as significant contributors in regulating pathways associated with T2D. Furthermore, these candidates exhibit potential as biomarkers for screening and diagnosing early onset, progression, and complications associated with T2D (Pordzik et al. [96]). Recent studies have demonstrated a significant association between the development and progression of T2D and the presence of hsa-mir-124–3p (Zhu et al. [97]). In this study, it was observed that hsa-mir-1-3p, hsa-mir-124–3p, and hsa-mir-155–5p exhibited the highest levels of expression among the microRNAs studied and these microRNAs demonstrated a more pronounced correlation with stevioside targeted DEGs.

Molecular docking approach was employed to verify the molecular interaction between stevioside and the common hub targets (*PPARG*, *PTGS2*, *PTPRC*, and *CXCL8*). The experimental findings revealed that most of hub targets exhibited distinct binding activity. Notably, *PPARG* demonstrated a binding energy of −8 kcal/mol, while *PTGS2* exhibited a stronger binding energy of −10.1 kcal/mol. These results suggest that

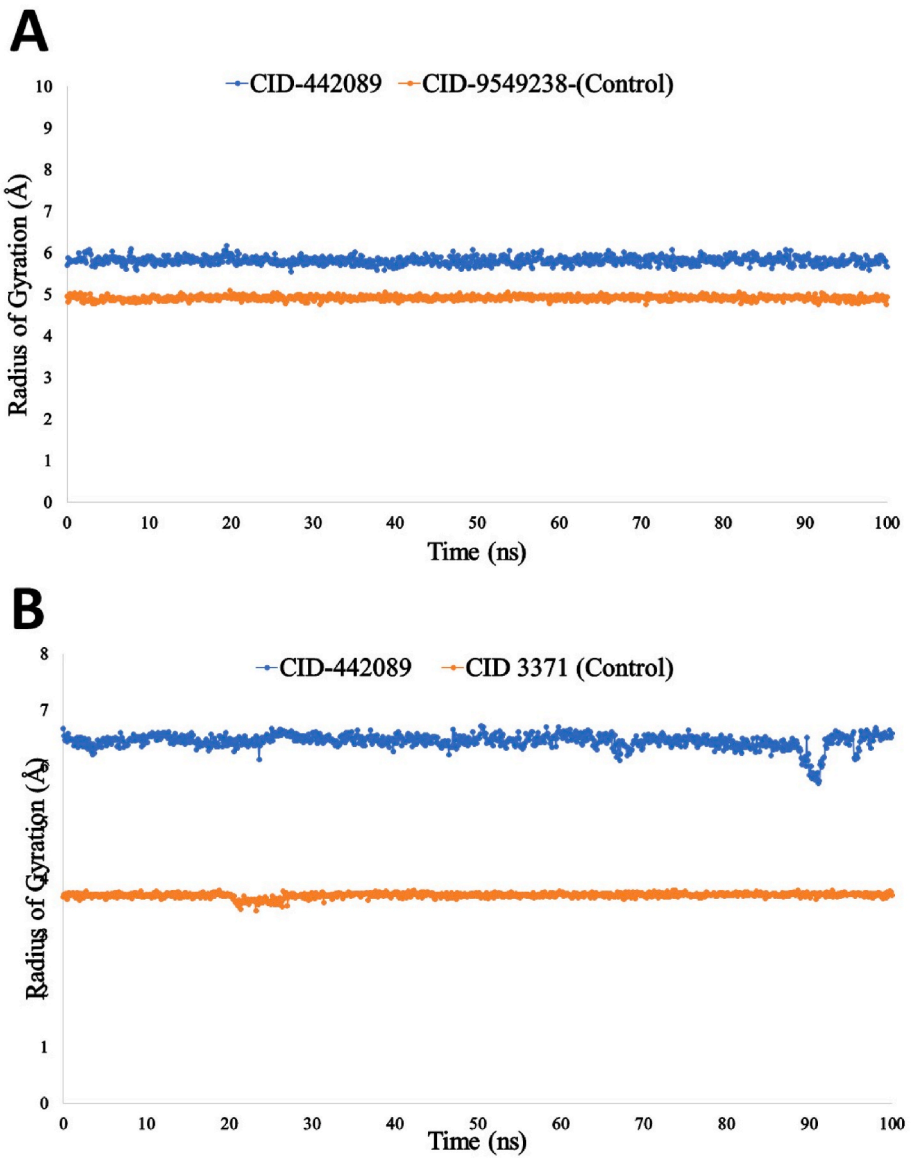

Fig. 12. The radius of gyration (Rg) values of 100 ns MDS assessment for the two ligand molecules in complex with the targeted protein (A) CID-442089 (stevioside) with *PPARG* (blue), CID- 9549238 (control) with *PPARG* (orange) and (B) CID-442089 (stevioside) with *PTGS2* (blue), CID- 3371 (control) with *PTGS2* (orange).

both *PPARG* and *PTGS2* have the capability to interact with their respective compounds tightly, indicating their potential significance in the management of T2D. Stabilizing the ligand at the binding interface is highly dependent on hydrophobic interactions. The targeted molecules may have many hydrophobic atoms to improve the drug-target interaction (Patil et al. [98]). The presence of hydrogen bonds increases the specificity of ligand binding (Wade et al. [99]). Our interaction study suggests hydrogen bonding and hydrophobicity are important considerations when developing a drug candidate for modulating *PPARG* and *PTGS2*.

Molecular dynamics for 100-ns was executed using the Schrodinger package software (Desmond Application), including relevant physicochemical and physiological parameters (Abdullah et al. [100]) to verify the stability of protein-ligand complexes. The structural compactness of complex can be determined by examining the RMSD value. The RMSF value is utilized to quantify the time-dependent variations in the protein-ligand complex (Shukla and Tripathi [101]). Within intricate systems, lower RMSD values imply the best stability of the compounds, while higher RMSF values suggest lower compactness of the protein-ligand complex (Saber et al. [102]). Stevioside (CID-442089) showed the potent RMSF and RMSD values with both the targeted proteins *PPARG* and *PTGS2* compared to the control drug. In the case of both *PPARG* and *PTGS2* proteins, a lower Rg value signifies a higher degree of compactness, while a higher Rg value indicates the dissociation of the compounds from the protein (Khan et al. [103]; Khan et al. [104]). Stevioside exhibited a slightly higher Rg value when compared to the control drug about the targeted proteins *PPARG* and *PTGS2*. In addition, the "Simulation Interaction Diagram" (SID) was employed to analyze the intermolecular interactions between proteins and specific ligands throughout a simulation period of 100 ns. The simulation revealed that the ligands formed multiple connections with the targeted proteins through hydrogen bonding, hydrophobic bonding, ionic bonding, and water bridge bonding. These connections persisted throughout the simulation, thereby promoting the establishment of stable binding between the ligands and the proteins. Furthermore, the MM/GBSA values suggest that stevioside maintains stable binding affinity with the specific protein targets *PPARG* and *PTGS2*.

The clinical relevance of the findings lies in the fact that previous research has indicated that thiazolidinediones (TZDs) such as rosiglitazone and pioglitazone preferentially focus on and stimulate *PPARG*,

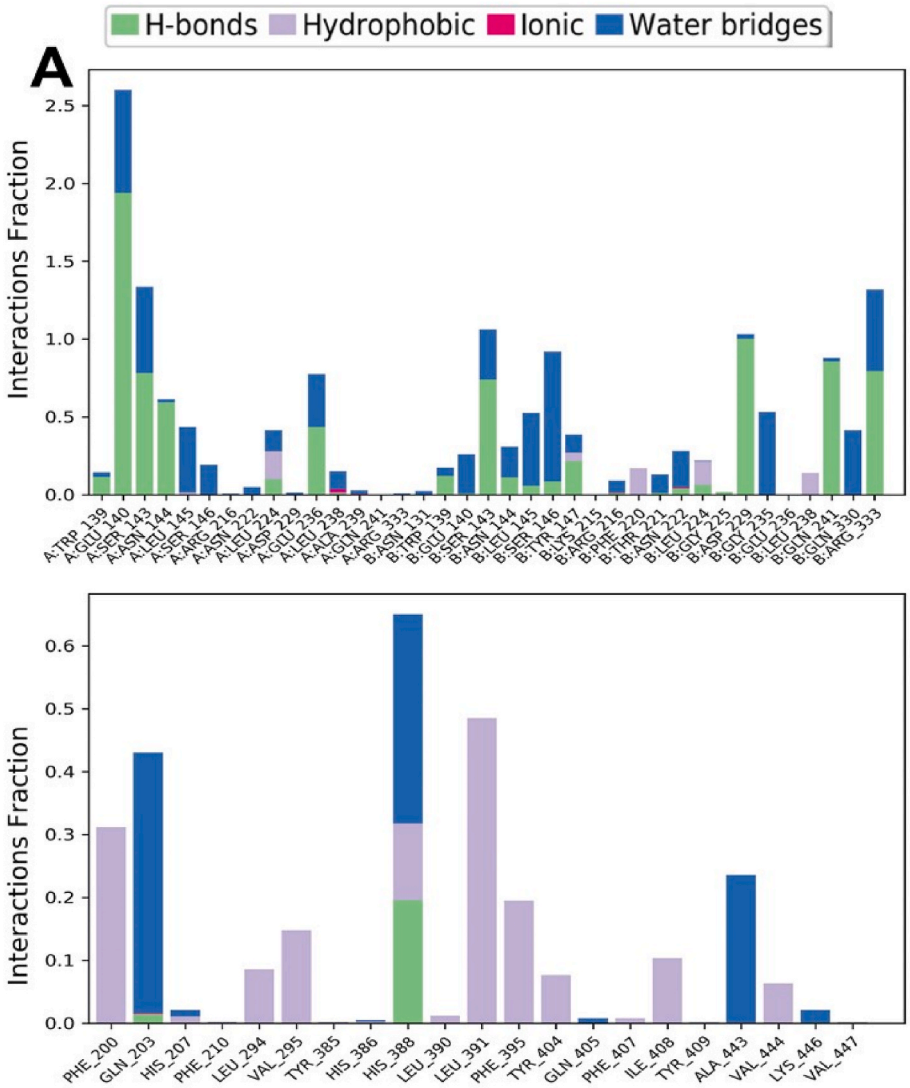

Fig. 13a. (**A**) The stacked bar charts represent protein-ligand intramolecular bond interactions during 100 ns simulation. The figure represents the interaction of two ligands with targeted protein *PTGS2,* where the top one is compound CID-442089 (stevioside), and the bottom one is the control drug CID-3371.

hence improving insulin sensitivity and glucose metabolism in individuals with T2D (Nanjan et al. [15]). Their usage is declining due to many adverse effects, including weight gain, fluid retention, and an elevated risk of heart failure (Won [105]). This study revealed that stevioside interacts with *PPARG* and *PTGS2*, which could also serve as therapeutic targets for controlling T2D. Stevioside has not yet been associated with any adverse effects (Sukhmani et al. [18]) and its cost-effective nature makes it an ideal prescription choice. Further *in-vivo* and *in-vitro* studies are needed to confirm target proteins as therapeutic targets of stevioside in controlling T2D. However, due to its potential benefits, clinicians may consider stevioside as an adjunct therapy for T2D. One study found that stevioside remains indigestible as it passes the upper gastrointestinal tract and converts to steviol when it encounters intestinal microflora. It is absorbed, and a large fraction is conjugated to steviol glucuronide in the liver, which also has an anti-hyperglycemic effect (Simoens et al. [106]). Future research should explore the potential interactions between steviol glucuronide with *PTGS2* and *PPARG* to elucidate its role in the management of T2D.

5. Conclusions

The research highlights the therapeutic potential of stevioside, in controlling T2D by targeting key molecular pathways and hub proteins. By integrating network pharmacology, molecular docking, and dynamics simulations, this study identified key molecular pathways and hub proteins, including *PPARG* and *PTGS2*, that stevioside targets in T2D management. Prostaglandin synthesis and regulation, IL-17 signaling, and inflammatory response are relevant pathways for T2D enriched by hub proteins. Network pharmacology analysis revealed the interaction of stevioside with six common hub proteins: *PPARG*, *PTGS2*, *PTPRC*, *CCL2*, *EDN1*, and *CXCL8*, which play significant roles in T2D. Molecular docking and dynamics simulations indicated that stevioside forms stable bonds with *PPARG* (−8 kcal/mol) and *PTGS2* (−10.1 kcal/mol). This investigation has contributed to the advancement of understanding regarding the specific target of stevioside for T2D, which holds potential significance in controlling and treating T2D. However, this analysis was primarily computational, further *in-vivo* and *in-vitro* experiments are needed to verify this *in-silico* study.

Limitations

The current study has certain limitations. The findings are based on the available data in the specified database. It is important to note that using various databases may lead to variations in the results. Hence,

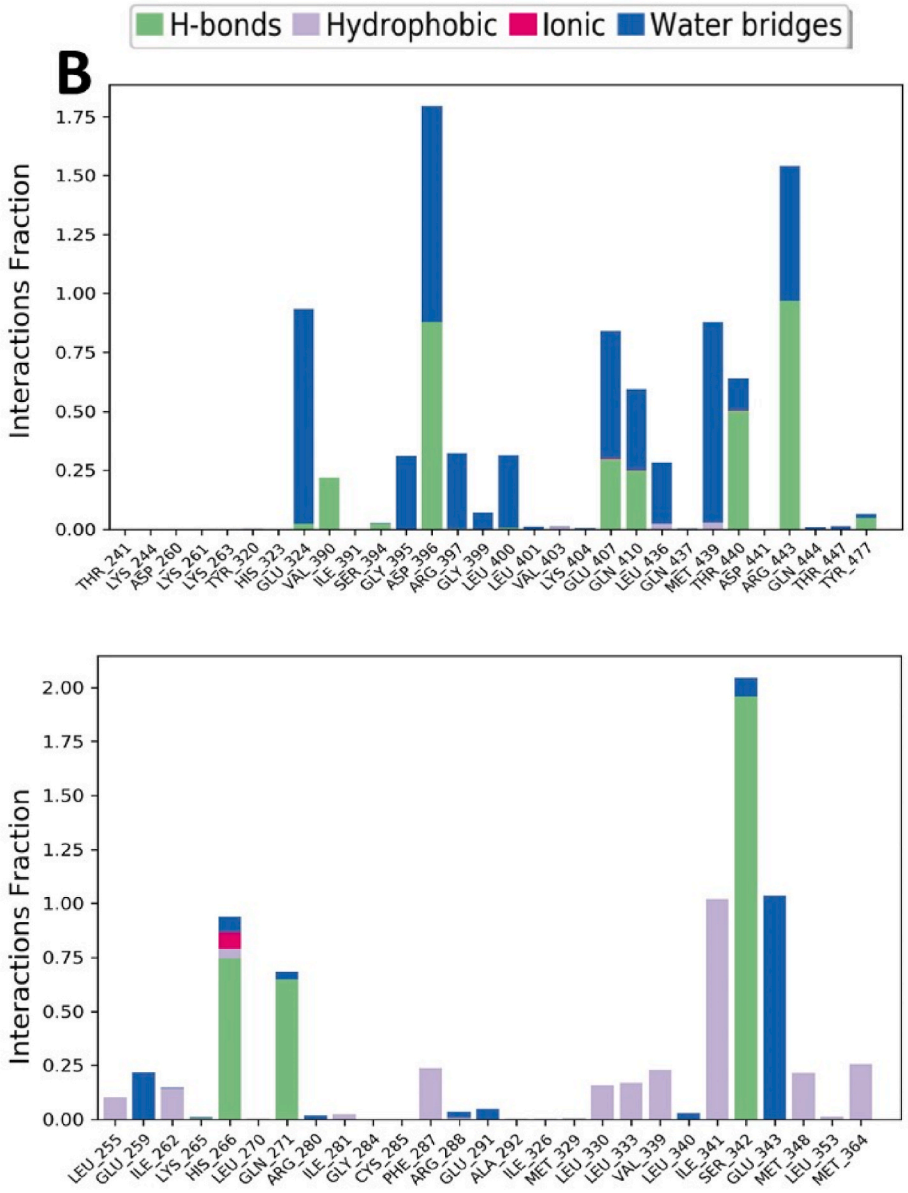

Fig. 13b. (**B**) The stacked bar charts represent protein-ligand intramolecular bond interactions during 100 ns simulation. The figure represents the interaction of two ligands with targeted protein *PPARG,* where top one is the compound CID-442089 (stevioside), and bottom one is the control drug CID-9549238.

further research should prioritize the multi-database analysis and regularly update databases. The sample size in this study was small, and one sample source was adipocyte tissue instead of pancreatic tissue. It is necessary to conduct more research to ensure the credibility of the conclusions drawn from this study. Therefore, further *in-vivo*, *in-vitro*, and clinical studies should be performed to verify this *in-silico* study.

Data availability statement

Data included in article/referenced in articles.

Additional information

Please find enclosed the supplementary file that includes supplementary information.

Conflict of interests

The authors declare that they have no known competing financial interests or personal relationships that could have appeared to influence the work reported in this paper.

Author contributions statement

Conceptualization was done by K.A., M.M.R., F.M.B.; Data curation, Formal analysis, Investigation, and Methodology by A.D., M.A.H., P.D.S., M.A.M.; Funding acquisition by M.M.R., F.M.B.; Project administration by K.A., M.M.R., F.M.B.; Resources, Software by P.D.S., M.A.M.; Supervision by M.M.R.; Validation by K.A., M.M.R., F.M.B.; Visualization and Writing of the original draft by A.D., M.A.H., P.D.S., M.A.M.; Writing: review editing by K.A., M.M.R., F.M.B.

Funding

This research work was funded by the Natural Sciences and Engineering Research Council of Canada (NSERC).

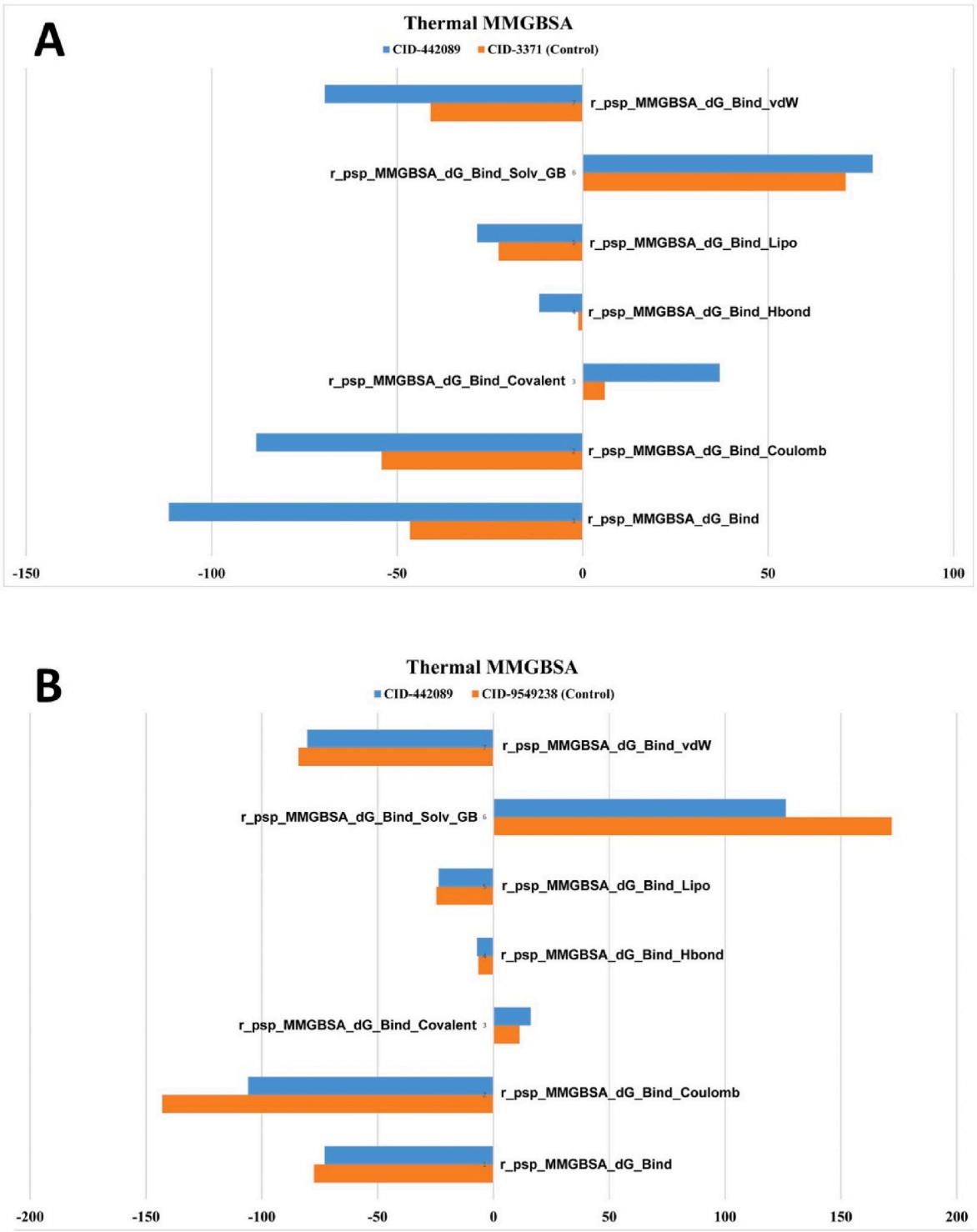

Fig. 14. The calculated average binding free energies (kcal/mol) for (A) *PTGS2* with compound CID-442089 (blue) and control drug CID-3371 (orange). (B) *PPARG* with compound CID-442089 (blue), and control drug CID-9549238 (orange).

Declaration of competing interest

The authors declare that they have no known competing financial interests or personal relationships that could have appeared to influence the work reported in this paper.

Appendix A. Supplementary data

Supplementary data to this article can be found online at https://doi.org/10.1016/j.dsx.2024.103111.

References

[1] De Candia P, et al. Type 2 diabetes: how much of an autoimmune disease? Front Endocrinol 2019;10:451.

[2] Rowley WR, Bezold C, Arikan Y, Byrne E, Krohe S. Diabetes 2030: insights from yesterday, today, and future trends. Popul Health Manag 2017;20(1):6–12.
[3] Galicia-Garcia U, et al. Pathophysiology of type 2 diabetes mellitus. Int J Mol Sci 2020;21(17):6275.
[4] Chen L, Magliano DJ, Zimmet PZ. The worldwide epidemiology of type 2 diabetes mellitus—present and future perspectives. Nat Rev Endocrinol 2012;8(4):228–36.
[5] Zatterale F, et al. Chronic adipose tissue inflammation linking obesity to insulin resistance and type 2 diabetes. Front Physiol 2020;10:505887.
[6] Gupta S, Tiwari M, Dubey V. Assessment of β-aescin effect in streptozotocin induced diabetic model: diabetic hepatotoxicity study. J. Pharm. Res. Int. 2021; 33(28A):160–8.
[7] Zheng Y, Ley SH, Hu FB. Global aetiology and epidemiology of type 2 diabetes mellitus and its complications. Nat Rev Endocrinol 2018;14(2):88–98.
[8] Reddy BM, Pranavchand R, Latheef SAA. Overview of genomics and post-genomics research on type 2 diabetes mellitus: future perspectives and a framework for further studies. J Bio Sci 2019;44(1):21. https://doi.org/10.1007/s12038-018-9818-6.
[9] Olokoba AB, Obateru OA, Olokoba LB. Type 2 diabetes mellitus: a review of current trends. Oman Med J Jul. 2012;27(4):269–73. https://doi.org/10.5001/omj.2012.68.
[10] Ismail-Beigi F, Moghissi E, Tiktin M, Hirsch IB, Inzucchi SE, Genuth S. Individualizing glycemic targets in type 2 diabetes mellitus: implications of recent clinical trials. Ann Intern Med 2011;154(8):554–9.
[11] Gæde P, Vedel P, Larsen N, Jensen GVH, Parving H-H, Pedersen O. Multifactorial intervention and cardiovascular disease in patients with type 2 diabetes. N Engl J Med Jan. 2003;348(5):383–93. https://doi.org/10.1056/NEJMoa021778.
[12] Yang R, et al. Cumulative blood pressure predicts risk of stroke in individuals with type 2 diabetes. Diabetes Metab. Syndr. Clin. Res. Rev. 2024;18(3):102988.
[13] Schalkwijk CG, Stehouwer CDA. Methylglyoxal, a highly reactive dicarbonyl compound, in diabetes, its vascular complications, and other age-related diseases. Physiol Rev 2020;100(1):407–61.
[14] Foretz M, Guigas B, Viollet B. Understanding the glucoregulatory mechanisms of metformin in type 2 diabetes mellitus. Nat Rev Endocrinol 2019;15(10):569–89.
[15] Nanjan MJ, Mohammed M, Kumar BRP, Chandrasekar MJN. Thiazolidinediones as antidiabetic agents: a critical review. Bioorg Chem 2018;77:548–67.
[16] Tey SL, Salleh NB, Henry J, Forde CG. Effects of aspartame-, monk fruit-, stevia- and sucrose-sweetened beverages on postprandial glucose, insulin and energy intake. Int J Obes 2017;41(3):450–7.
[17] Eddouks M, Bidi A, El Bouhali B, Hajji L, Zeggwagh NA. Antidiabetic plants improving insulin sensitivity. J Pharm Pharmacol 2014;66(9):1197–214.
[18] Ilić V, Vukmirović S, Stilinović N, Čapo I, Arsenović M, Milijašević B. Insight into anti-diabetic effect of low dose of stevioside. Biomed Pharmacother 2017;90: 216–21.
[19] Sukhmani G, Yogesh G, Shalini A, Vikas K, Anil P, Ashwani K. Natural sweeteners: health benefits of stevia. Foods raw Mater 2018;6(2):392–402.
[20] Assaei R, et al. Hypoglycemic effect of aquatic extract of Stevia in pancreas of diabetic rats: PPARγ-dependent regulation or antioxidant potential. Avicenna J Med Biotechnol (AJMB) 2016;8(2):65.
[21] Jeppesen PB, Gregersen S, Poulsen CR, Hermansen K. Stevioside acts directly on pancreatic β cells to secrete insulin: actions independent of cyclic adenosine monophosphate and adenosine triphosphate—sensitivie K+-channel activity. Metabolism 2000;49(2):208–14.
[22] Potočnjak I, Broznić D, Kindl M, Kropek M, Vladimir-Knežević S, Domitrović R. Stevia and stevioside protect against cisplatin nephrotoxicity through inhibition of ERK1/2, STAT3, and NF-κB activation. Food Chem Toxicol 2017;107:215–25.
[23] Boonkaewwan C, Toskulkao C, Vongsakul M. Anti-inflammatory and immunomodulatory activities of stevioside and its metabolite steviol on THP-1 cells. J Agric Food Chem 2006;54(3):785–9.
[24] Alavala S, et al. Stevioside, a diterpenoid glycoside, shows anti-inflammatory property against Dextran Sulphate Sodium-induced ulcerative colitis in mice. Eur J Pharmacol 2019;855:192–201.
[25] Wan J, et al. Stevioside protects primary articular chondrocytes against IL-1β-induced inflammation and catabolism by targeting integrin. Int Immunopharm 2023;119:110261.
[26] Hao W, Yu T, Zuo D, Hu H, Zhou P. Stevioside attenuates bleomycin-induced pulmonary fibrosis by activating the Nrf2 pathway and inhibiting the NF-κB and TGF-β1/Smad2/3 pathways. Exp Lung Res 2023;49(1):205–19.
[27] Casas-Grajales S, et al. Antioxidant and immunomodulatory activity induced by stevioside in liver damage: in vivo, in vitro and in silico assays. Life Sci 2019;224: 187–96.
[28] Chen J, Jeppesen PB, Nordentoft I, Hermansen K. Stevioside counteracts the glyburide-induced desensitization of the pancreatic beta-cell function in mice: studies in vitro. Metabolism 2006;55(12):1674–80. https://doi.org/10.1016/j.metabol.2006.08.009.
[29] Chen T-H, Chen S-C, Chan P, Chu Y-L, Yang H-Y, Cheng J-T. Mechanism of the hypoglycemic effect of stevioside, a glycoside of Stevia rebaudiana. Planta Med 2005;71(2):108–13.
[30] Stupnikov A, et al. Robustness of differential gene expression analysis of RNA-seq. Comput Struct Biotechnol J 2021;19:3470–81. https://doi.org/10.1016/j.csbj.2021.05.040.
[31] Davis AP, et al. The comparative toxicogenomics database: update 2019. Nucleic Acids Res 2019;47(D1):D948–54.
[32] Hewett M, et al. PharmGKB: the pharmacogenetics knowledge base. Nucleic Acids Res 2002;30(1):163–5.
[33] Kuhn M, von Mering C, Campillos M, Jensen LJ, Bork P. STITCH: interaction networks of chemicals and proteins. Nucleic Acids Res 2007;36(suppl_1):D684–8.
[34] Wang X, et al. PharmMapper 2017 update: a web server for potential drug target identification with a comprehensive target pharmacophore database. Nucleic Acids Res 2017;45(W1):W356–60.
[35] Gfeller D, Grosdidier A, Wirth M, Daina A, Michielin O, Zoete V. SwissTargetPrediction: a web server for target prediction of bioactive small molecules. Nucleic Acids Res 2014;42(W1):W32–8.
[36] Gaulton A, et al. ChEMBL: a large-scale bioactivity database for drug discovery. Nucleic Acids Res 2012;40(D1):D1100–7.
[37] Geer LY, et al. The NCBI biosystems database. Nucleic Acids Res 2010;38(suppl_1):D492–6.
[38] Kaussner A, Grein M, Krüger H-P, Noltemeier H. In: An architecture for driving simulator databases with generic and dynamically changing road networks; 2001.
[39] Rahman MH, et al. Bioinformatics and system biology approaches to identify pathophysiological impact of COVID-19 to the progression and severity of neurological diseases. Comput Biol Med 2021;138:104859.
[40] Oliveros JC. In: VENNY. An interactive tool for comparing lists with Venn Diagrams; 2007. bioinfogp.cnb.csic.es/tools/venny/index.html.
[41] Kanehisa M. The KEGG database. In: In Silico˙Simulation of biological processes: novartis foundation symposium, vol. 247; 2002. p. 91–103. 247.
[42] Belenahalli Shekarappa S, Kandagalla S, Hanumanthappa M. A network pharmacology approach to investigate the pharmacological effect of curcumin and capsaicin targets in cancer angiogenesis by module-based PPI network analysis. J Protein Proteonomics 2019;10:109–20.
[43] Darbeheshti F, Rezaei N, Amoli MM, Mansoori Y, Tavakkoly Bazzaz J. Integrative analyses of triple negative dysregulated transcripts compared with non-triple negative tumors and their functional and molecular interactions. J Cell Physiol 2019;234(12):22386–99.
[44] Wang J, Zhong J, Chen G, Li M, Wu F, Pan Y. ClusterViz: a cytoscape APP for cluster analysis of biological network. IEEE ACM Trans Comput Biol Bioinf 2014; 12(4):815–22.
[45] Chin C-H, Chen S-H, Wu H-H, Ho C-W, Ko M-T, Lin C-Y. cytoHubba: identifying hub objects and sub-networks from complex interactome. BMC Syst Biol 2014;8 (4):1–7.
[46] Bardou P, Mariette J, Escudié F, Djemiel C, Klopp C. jvenn: an interactive Venn diagram viewer. BMC Bioinf 2014;15(1):1–7.
[47] Zhou G, Soufan O, Ewald J, Hancock REW, Basu N, Xia J. NetworkAnalyst 3.0: a visual analytics platform for comprehensive gene expression profiling and meta-analysis. Nucleic Acids Res 2019;47(W1):W234–41.
[48] Fornes O, Castro-Mondragon JA, Khan A, van der Lee R, Zhang X, Richmond PA, Modi BP, Correard S, Gheorghe M, Baranasic D, Santana-Garcia W, Tan G, Cheneby J, Ballester B, Parcy F, Sandelin A, Lenhard B, Wasserman WW, Mathelier A. JASPAR 2020: update of the open-access database of transcription factor binding profiles. Nucleic Acids Res 2020;48(D1):D87–92.
[49] Sloan CA, et al. ENCODE data at the ENCODE portal. Nucleic Acids Res 2016;44 (D1):D726–32.
[50] Papadopoulos GL, Reczko M, Simossis VA, Sethupathy P, Hatzigeorgiou AG. The database of experimentally supported targets: a functional update of TarBase. Nucleic Acids Res 2009;37(suppl_1):D155–8.
[51] Hsu S-D, et al. miRTarBase: a database curates experimentally validated microRNA–target interactions. Nucleic Acids Res 2011;39(suppl_1):D163–9.
[52] Guedes IA, de Magalhães CS, Dardenne LE. Receptor–ligand molecular docking. Biophys. Rev. 2014;6:75–87.
[53] Rose PW, et al. The RCSB protein data bank: integrative view of protein, gene and 3D structural information. Nucleic Acids Res 2016:gkw1000.
[54] Guex N, Peitsch MC, Schwede T. Automated comparative protein structure modeling with SWISS-MODEL and Swiss-PdbViewer: a historical perspective. Electrophoresis 2009;30(S1):S162–73.
[55] Tian W, Chen C, Lei X, Zhao J, Liang J. CASTp 3.0: computed atlas of surface topography of proteins. Nucleic Acids Res Jul. 2018;46(W1):W363–7. https://doi.org/10.1093/nar/gky473.
[56] Kim S, et al. PubChem substance and compound databases. Nucleic Acids Res 2016;44(D1):D1202–13.
[57] Nivetha R, Bhuvaragavan S, Muthu Kumar T, Ramanathan K, Janarthanan S. Inhibition of multiple SARS-CoV-2 proteins by an antiviral biomolecule, seselin from Aegle marmelos deciphered using molecular docking analysis. J Biomol Struct Dyn 2022;40(21):11070–81.
[58] Dallakyan S, Olson AJ. Small-molecule library screening by docking with PyRx. Methods Mol Biol 2015. https://doi.org/10.1007/978-1-4939-2269-7_19.
[59] Arefin A, et al. Target specificity of selective bioactive compounds in blocking α-dystroglycan receptor to suppress Lassa virus infection: an in silico approach. J. Biomed. Res. 2021;35(6):459.
[60] Biswas P, et al. Analysis of SYK gene as a prognostic biomarker and suggested potential bioactive phytochemicals as an alternative therapeutic option for colorectal cancer: an in-silico pharmaco-informatics investigation. J Personalized Med 2021;11(9):888.
[61] Roos K, et al. OPLS3e: Extending force field coverage for drug-like small molecules. J Chem Theor Comput 2019;15(3):1863–74.
[62] Rahman MS, et al. In vivo neuropharmacological potential of gomphandra tetrandra (wall.) sleumer and in-silico study against β-amyloid precursor protein. Processes 2021;9(8):1449.
[63] El Khoury L, et al. In: The D3R grand challenge, vol. 4; 2019.
[64] Zarezade V, et al. The identification of novel inhibitors of human angiotensin-converting enzyme 2 and main protease of Sars-Cov-2: a combination of in silico methods for treatment of COVID-19. J Mol Struct 2021;1237:130409.

[65] Du J, Wang X, Nie Q, Yang J, Yao X. Computational study of the binding mechanism of medium chain acyl-CoA synthetase with substrate in Methanosarcina acetivorans. J Biotechnol 2017;259:160–7.
[66] Zarezade V, Abolghasemi M, Rahim F, Veisi A, Behbahani M. In silico assessment of new progesterone receptor inhibitors using molecular dynamics: a new insight into breast cancer treatment. J Mol Model 2018;24:1–19.
[67] Safavi A, et al. Computational investigation of novel farnesyltransferase inhibitors using 3D-QSAR pharmacophore modeling, virtual screening, molecular docking and molecular dynamics simulation studies: a new insight into cancer treatment. J Mol Struct 2021;1241:130667.
[68] AbdElmoniem N, et al. Identification of novel natural dual HDAC and Hsp90 inhibitors for metastatic TNBC using e-pharmacophore modeling, molecular docking, and molecular dynamics studies. Molecules 2023;28(4):1771.
[69] Sonnweber T, Pizzini A, Nairz M, Weiss G, Tancevski I. Arachidonic acid metabolites in cardiovascular and metabolic diseases. Int J Mol Sci 2018;19(11). https://doi.org/10.3390/ijms19113285.
[70] Luo P, Wang M-H. Eicosanoids, β-cell function, and diabetes. Prostag Other Lipid Mediat 2011;95(1):1–10. https://doi.org/10.1016/j.prostaglandins.2011.06.001.
[71] Kimple ME, et al. Prostaglandin E2 receptor, EP3, is induced in diabetic islets and negatively regulates glucose- and hormone-stimulated insulin secretion. Diabetes May 2013;62(6):1904–12. https://doi.org/10.2337/db12-0769.
[72] Carboneau BA, Allan JA, Townsend SE, Kimple ME, Breyer RM, Gannon M. Opposing effects of prostaglandin E2 receptors EP3 and EP4 on mouse and human β-cell survival and proliferation. Mol Metabol 2017;6(6):548–59. https://doi.org/10.1016/j.molmet.2017.04.002.
[73] Bosma KJ, Kaiser CE, Kimple ME, Gannon M. Effects of arachidonic acid and its metabolites on functional beta-cell mass. Metabolites 2022;12(4). https://doi.org/10.3390/metabo12040342.
[74] Odegaard AO, Jacobs DR, Sanchez OA, Goff DC, Reiner AP, Gross MD. Oxidative stress, inflammation, endothelial dysfunction and incidence of type 2 diabetes. Cardiovasc Diabetol 2016;15:1–12.
[75] Elahi R, Nazari M, Mohammadi V, Esmaeilzadeh K, Esmaeilzadeh A. In: IL-17 in type II diabetes mellitus (T2DM) immunopathogenesis and complications; molecular approaches; 2023.
[76] Abdel-Moneim A, Bakery HH, Allam G. The potential pathogenic role of IL-17/Th17 cells in both type 1 and type 2 diabetes mellitus. Biomed Pharmacother 2018;101:287–92. https://doi.org/10.1016/j.biopha.2018.02.103.
[77] Zaharieva E, Kamenov Z, Velikova T, Tsakova A, El-Darawish Y, Okamura H. Interleukin-18 serum level is elevated in type 2 diabetes and latent autoimmune diabetes. Endocr. Connect. 2018;7(1):179–85.
[78] Iordanidou M, et al. The serotonin transporter promoter polymorphism (5-HTTLPR) is associated with type 2 diabetes. Clin Chim Acta 2010;411(3–4):167–71.
[79] Konheim YL, Wolford JK. Association of a promoter variant in the inducible cyclooxygenase-2 gene (PTGS2) with type 2 diabetes mellitus in Pima Indians. Hum Genet 2003;113:377–81.
[80] Chen Q, et al. LncRNA PTGS2 regulates islet β-cell function through the miR-146a-5p/RBP4 axis and its diagnostic value in type 2 diabetes mellitus. Am. J. Transl. Res. 2021;13(10):11316.
[81] Yingkun N, Zhenyu W, Jing L, Xiuyun L, Huimin Y. Stevioside protects LPS-induced acute lung injury in mice. Inflammation 2013;36:242–50.
[82] Hong J, Chen L, Jeppesen PB, Nordentoft I, Hermansen K. Stevioside counteracts the α-cell hypersecretion caused by long-term palmitate exposure. Am. J. Physiol. Metab 2006;290(3):E416–22.
[83] Mal S, Dwivedi AR, Kumar V, Kumar N, Kumar B, Kumar V. Role of peroxisome proliferator-activated receptor gamma (PPARγ) in different disease states: recent updates. Curr Med Chem 2021;28(16):3193–215.
[84] Longo M, et al. Adipose tissue dysfunction as determinant of obesity-associated metabolic complications. Int J Mol Sci 2019;20(9):2358.
[85] Wang L, et al. Natural product agonists of peroxisome proliferator-activated receptor gamma (PPARγ): a review. Biochem Pharmacol 2014;92(1):73–89.
[86] Ahmadian M, et al. PPARγ signaling and metabolism: the good, the bad and the future. Nat Med 2013;19(5):557–66.
[87] Lalloyer F, Staels B. Fibrates, glitazones, and peroxisome proliferator–activated receptors. Arterioscler Thromb Vasc Biol 2010;30(5):894–9.
[88] Zhang Y. Mechanism of neuroprotective effect of stevioside on cerebral ischemia-reperfusion injury via PPAR-γ activation. Immunopharmacol Immunotoxicol 2021;43(6):704–12.
[89] Bruun JM, et al. Higher production of IL-8 in visceral vs. subcutaneous adipose tissue. Implication of nonadipose cells in adipose tissue. Am. J. Physiol. Metab 2004;286(1):E8–13.
[90] Straczkowski M, Dzienis-Straczkowska S, Stepien A, Kowalska I, Szelachowska M, Kinalska I. Plasma interleukin-8 concentrations are increased in obese subjects and related to fat mass and tumor necrosis factor-α system. J Clin Endocrinol Metab 2002;87(10):4602–6.
[91] Hermiston ML, Xu Z, Weiss A. CD45: a critical regulator of signaling thresholds in immune cells. Annu Rev Immunol 2003;21(1):107–37.
[92] Prabhakar PK, Sivakumar PM. Protein tyrosine phosphatase 1B inhibitors: a novel therapeutic strategy for the management of type 2 diabetes mellitus. Curr Pharmaceut Des 2019;25(23):2526–39.
[93] Omatsu T, et al. CXCL1/CXCL8 (GROα/IL-8) in human diabetic ketoacidosis plasma facilitates leukocyte recruitment to cerebrovascular endothelium in vitro. Am. J. Physiol. Metab 2014;306(9):E1077–84.
[94] Muiya NP, et al. A study of the role of GATA2 gene polymorphism in coronary artery disease risk traits. Gene 2014;544(2):152–8.
[95] Liu D, et al. YY1 regulates glucose homeostasis through controlling insulin transcription in pancreatic β-cells. Diabetes 2022;71(5):961–77.
[96] Pordzik J, et al. Significance of circulating microRNAs in diabetes mellitus type 2 and platelet reactivity: bioinformatic analysis and review. Cardiovasc Diabetol 2019;18:1–19.
[97] Zhu Z, Yin J, Li DC, Mao ZQ. Role of microRNAs in the treatment of type 2 diabetes mellitus with Roux-en-Y gastric bypass. Braz J Med Biol Res 2017;50.
[98] Patil R, Das S, Stanley A, Yadav L, Sudhakar A, Varma AK. Optimized hydrophobic interactions and hydrogen bonding at the target-ligand interface leads the pathways of drug-designing. PLoS One 2010;5(8):e12029.
[99] Wade RC, Goodford PJ. The role of hydrogen-bonds in drug binding. Prog Clin Biol Res 1989;289:433–44.
[100] Abdullah A, et al. Molecular dynamics simulation and pharmacoinformatic integrated analysis of bioactive phytochemicals from Azadirachta indica (neem) to treat diabetes mellitus. J Chem 2023;2023.
[101] Shukla R, Tripathi T. Molecular dynamics simulation of protein and protein–ligand complexes. Comput. drug Des. 2020:133–61.
[102] Al Saber M, et al. A comprehensive review of recent advancements in cancer immunotherapy and generation of CAR T cell by CRISPR-Cas9. Processes 2021;10(1):16.
[103] Khan RA, et al. Diterpenes/diterpenoids and their derivatives as potential bioactive leads against dengue virus: a computational and network pharmacology study. Molecules 2021;26(22):6821.
[104] Khan AM, et al. In vitro and in silico investigation of garlic's (Allium sativum) bioactivity against 15-lipoxygenase mediated inflammopathies. J. Herbmed Pharmacol. 2023;12(2):283–98.
[105] Won JC. Thiazolidinediones (TZDs). Stroke Revisit. Diabetes Stroke 2021:131–41.
[106] Simoens C, et al. Steviol, the aglycon of steviol glycosides, does not reduce hyperglycemia in mice with type 2 diabetes. Phytomedicine 2022;2(4):100362.
[107] Dhananjayan R, Koundinya KSS, Malati T, Kutala VK. Endothelial dysfunction in type 2 diabetes mellitus. Indian J Clin Biochem 2016;31:372–9.
[108] Al Barashdi MA, Ali A, McMullin MF, Mills K. Protein tyrosine phosphatase receptor type C (PTPRC or CD45). J Clin Pathol 2021;74(9):548–52.
[109] Kim K-W, Ivanov S, Williams JW. Monocyte recruitment, specification, and function in atherosclerosis. Cells 2020;10(1):15.